

# **Kinetic controls on the thermometry of mantle rocks: A case study from the Xigaze Ophiolites, Tibet**

L. ZHAO and S. CHAKRABORTY

*Institut für Geologie, Mineralogie und Geophysik, Ruhr Universität  
Bochum, Bochum, Germany*

Temperature-dependent equilibrium partitioning of elements between different mineral (or melt/glass) phases forms the basis of geothermometry. In natural rock systems it is necessary to determine whether equilibrium partitioning of a given element was obtained between two phases before calculating temperatures using the tool. With the improvement of spatial resolution of analytical tools and our understanding of solid-state kinetics it has become clear that compositional heterogeneities on different scales exist in mantle rocks because of incomplete equilibration, and a kinetic evaluation is necessary before application of geothermometers. This work summarizes the kinetic situations that may arise and provides some guidelines and criteria for testing whether partitioning equilibrium was obtained. A suite of dunites and harzburgites from an ophiolite suite in the Himalaya (Xigaze, Tibet) is used to illustrate the application of some of these concepts. It is shown that when compositions used for geothermometry are chosen bearing these kinetic considerations in mind, a systematic pattern of freezing temperatures is obtained from the geothermometers. These data provide insights into the cooling histories of these rocks with complex, multistage (e.g. melt percolation) histories. Some potential pitfalls for geospeedometry are also illustrated along the way.

## **1. Introduction**

Petrological analysis has evolved from the study of rocks to understand the condition of formation to a recognition that rocks record a ‘chain of processes’ that took place in the course of their evolution through different pressure-temperature conditions. So, the question becomes: when does a given geothermometer/barometer ‘freeze’, and at what stage in the history of the rock does it record? Conventionally, thermobarometry has been studied largely in the domain of thermodynamics, but with this expanded view, kinetics plays as much of a role. As thermobarometry becomes a freezing issue rather than just a phase equilibrium problem, one has to ask, for example, the question: Which compositions were in equilibrium with each other (i.e. what should be measured and combined with each other) to get pressures and temperatures? Equilibrium calculations do not depend on the history of a system, and consideration of only the phases and components involved in the equilibrium process determine the system completely. Kinetics, on the other hand, does depend on pathways of processes (e.g. through initial- and boundary-conditions mechanisms of reaction). Therefore, the practice of thermobarometry becomes dependent on the nature and behaviour of the surrounding medium in addition to those involved directly in the equilibrium of interest, and the temperatures that are

obtained from different element exchange geothermometers depend on the kinetics of element exchange between the mineral phases concerned.

Generally, the differences between freezing temperatures are amplified for slower cooling rates. Element exchange thermometry of mantle rocks is an important tool for reconstructing the thermal history of different processes in the mantle. Compared to rapidly ascended xenoliths, the role of kinetics is more pronounced in the slowly cooled and emplaced mantle segments in ophiolites. On the one hand, the spatial context provided by different lithological units within an ophiolite sequence provide additional information and an internal check of methods. On the other hand, mineral pairs within rocks in an ophiolite sequence are affected by multiple events (= thermal pulses) that result from percolating melts that affect the phase assemblages and compositional distributions; and these need to be considered in the determination of compositions for and interpretation of the results of thermometry. Thus mantle ophiolite sequences provide some challenges as well as unique opportunities to study the kinetic controls on thermometry. Here, after outlining the principles of element exchange thermometry and some of the kinetic controls that govern element exchange we present an illustration using samples from the Xigaze ophiolite in Tibet. The implications of the results also include aspects about the application of geospeedometry to such mantle rocks.

## 2. Thermodynamics of thermobarometry and the role of kinetics

If two elements ( $i$  and  $j$ ) interchange between phases  $\alpha$  and  $\beta$  by the reaction:  $i-\alpha + j-\beta \leftrightarrow j-\alpha + i-\beta$ , then  $K_D$  is defined as the ratio of the two exchanged elements in one phase times the inverse ratio of the two exchanged elements in the other phase (equation 1).

$$K_D = \frac{X_i^\alpha * X_j^\beta}{X_j^\alpha * X_i^\beta}, \text{ where } X_i^\alpha = i/(i+j) \quad (1)$$

$K_D$  at equilibrium is a function of only  $P$  and  $T$  in thermodynamically ideal systems, and is a function of composition as well in non-ideal systems. The temperature dependence of  $K_D$  in the form  $\ln K_d = A/T + B + C(X)$ , is used as a thermometer. Here  $A$  and  $B$  are constants the values of which depend on the identities of  $i, j, \alpha$  and  $\beta$ ;  $C(X)$  appears only in non-ideal systems and may have complex functional forms. Conventionally, the compositions  $X_i^\alpha$  are measured in a sample to calculate a  $K_D$  which is then compared to an experimental (or model) calibration of the same as a function of temperature to determine the temperature of the natural sample. The underlying assumption of this exercise is that the measured compositions in the natural sample represent a frozen equilibrium state at some point in the history of the sample. In the event where multiple compositions of the same mineral are found in a sample (either as compositional zoning within individual grains; or as different grains, often in different textural locations), a process of kinetic evaluation is necessary to determine

which compositions to pair with which others, and whether any of the compositions were in equilibrium with each other.

Two relationships derived from the above, that are useful (Ganguly and Saxena, 1987) are:

$$X_i^\alpha = \frac{X_i^\beta}{K_D(1 - X_i^\beta) + X_i^\beta} \quad (2)$$

$$X_i^\beta = \frac{K_D * X_i^\alpha}{X_i^\alpha(K_D - 1) + 1} \quad (3)$$

These equations hold if both phases ( $\alpha$  and  $\beta$ ) are ideal solutions; again, additional terms appear in non-ideal systems but the general behaviour may still be studied with the help of these equations. Kinetic tests essentially involve checking if equations 2 and 3 are satisfied. Towards this end, Roozeboom diagrams that plot compositional pairs  $X_i^\alpha$  vs.  $X_i^\beta$  are a valuable aid. Indeed, these have been used since the early days of applications of thermodynamics in petrology to demonstrate that phase equilibrium is obtained among natural mineral assemblages and thermodynamics may be applied at all (Ganguly and Saxena, 1987; see Ganguly, 2021, for a historical perspective). In such a plot, calibration curves at different temperatures that were used to develop a thermometer (e.g. from experiments or a model) are plotted. Compositional pairs  $X_i^\alpha$  vs.  $X_i^\beta$  that plot on or adjacent to these curves indicate that those analyses could be either in or approaching equilibrium. On the other hand, a scatter (or plot outside the domain of calibrated curves) indicates that element exchange equilibrium was not achieved and these compositions should not be used for thermometry (examples are provided in the case study below). The Roozeboom diagram of  $X_i^\alpha$  vs.  $X_i^\beta$  would be symmetrical with reference to the intersection diagonal in ideal solutions at a given constant  $P$  and  $T$ . Other criteria in addition to consistency in a Roozeboom diagram are necessary for a complete kinetic test; these are discussed in the next section.

Fe-Mg exchange between many mineral pairs have been calibrated as geothermometers and the following are used in the illustrative examples with dunites and harzburgites below: orthopyroxene-clinopyroxene (Ganguly *et al.*, 2013), olivine-clinopyroxene (Kawasaki and Ito, 1994), olivine-orthopyroxene (von Seckendorff and O'Neill, 1993), spinel-olivine (Ballhaus *et al.*, 1991) and spinel-orthopyroxene (Liermann and Ganguly, 2003). The thermometers are usually temperature dependent and are insensitive to pressure. For example, the temperature variation is  $<2^\circ\text{C}/\text{kbar}$  and  $4^\circ\text{C}/\text{kbar}$  for spinel-olivine (Ballhaus *et al.*, 1991) and spinel-orthopyroxene (Liermann and Ganguly, 2003) Fe-Mg exchange thermometers respectively. In addition to these, the REE in the two-pyroxene thermometer of Liang *et al.* (2013) has been used in the present study.

### 3. Kinetics of Thermobarometry

The main change that occurs due to the entry of kinetics into the practice of thermobarometry is that spatial (= textural) context becomes important. This manifests itself in various forms ranging from the need to identify reaction textures, through identification of different generations of minerals, to the appropriate selection of compositions to use for thermobarometry from a compositionally zoned mineral. As the spatial disposition of mineral grains controls kinetics, different situations arise depending on the properties and geometric disposition of the grains and their surrounding medium. Compositional readjustment during cooling from some peak temperature in the absence of growth-dissolution have been considered in several models that considered primarily diffusion in mineral grains (e.g. Dodson, 1973; Dodson, 1976; Dodson, 1986; Eiler *et al.*, 1991; Lasaga, 1983). Four broad types of situations may be recognized: (1) a mineral grain is embedded in a matrix with which unrestrained (i.e. enough solubility and diffusivity in the matrix) exchange is possible, and for thermobarometry/geospeedometry-only analyses from this one mineral is necessary; (2) two mineral grains exchanging elements are in contact with each other (and “leakage” via the contact grain boundary to other minerals is negligible/limited); (3) two mineral grains that are not in contact with each other and exchange elements through a “grain boundary medium”, but transport via this medium is fast and unhindered (the ‘fast grain boundary model’); and (4) the most general case where the two mineral grains are not in contact with each other and exchange elements through a grain boundary, but the properties of the grain boundary (ability to contain the element of interest, transport rates, length, etc.) are also considered explicitly (Fig. 1).

(i) **Kinetics of compositional preservation during cooling in a mineral grain embedded in a matrix with unrestrained transport:** The formulations for this situation are due to Dodson (1973, 1976, 1986). There is a general misconception that these relate to diffusion-controlled processes only. The general form of the Dodson equation (Dodson, 1976) is

$$T_c = \frac{E}{R \ln\left(-\tau \frac{k_0}{a}\right)} \quad (4)$$

where  $T_c$  is the temperature at which a mineral composition freezes,  $R$  is the gas constant,  $k_0$  is a pre-exponential factor and  $E$  the activation energy for ‘any kinetic process that follows an Arrhenius type of law’ of temperature dependence,  $a$  is a geometric parameter and  $\tau$  is a characteristic (cooling) time constant. The more commonly seen formulation is where the kinetic parameters have been replaced explicitly by parameters related to diffusion. As can be seen from the expression, there are no provisions for accounting for the behaviour of the matrix (no terms that describe the behaviour in the matrix) or for different initial conditions (i.e. conditions far removed from the initial condition so that the initial condition is not preserved anywhere in the crystal). Modifications that

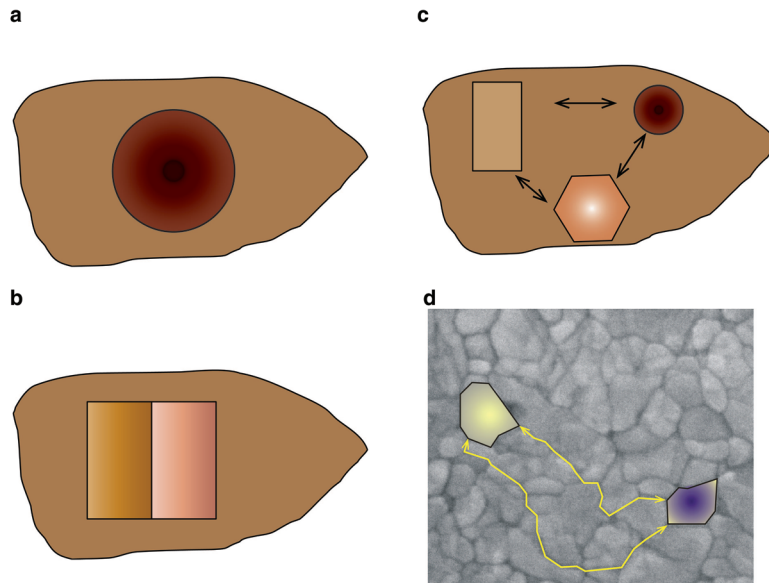


**Fig. 1.** Schematic representation of various models of kinetics of element exchange. **(a)** The Dodson model, where a crystal (dark brown sphere) exchanges elements with a matrix (lighter brown) where transport is unrestricted. **(b)** Geospeedometry element exchange model of Lasaga (1983) where two crystals (rectangular prisms of different colours in the middle), with colour gradation to represent compositional zoning that develops during cooling. The surrounding matrix, isolated in this case from the exchanging crystal-pair, is depicted in the same light brown shade as in **(a)**. **(c)** Fast grain boundary model of Eiler *et al.* (1991, 1992) and Jenkins *et al.* (1994) where multiple crystals sit in a matrix (light brown) physically separated from each other and communicate (= exchange elements) with each other via grain boundaries through which transport is fast and unrestricted. Colour gradation represents compositional zoning. **(d)** The Dohmen and Chakraborty model where two crystals that are physically separated from each other (yellow and blue) exchange elements with each other via a grain boundary network which has its own properties (solubility, diffusion rates for different elements as well as geometrical features such as length and surface area of contact). Colour gradation represents compositional zoning again.

account for some of these aspects have been developed (e.g. Ganguly and Tirone, 1999) that allow the formulation to be used in some cases. But the fact that the exchange partner is not considered explicitly makes the formulation of somewhat limited use and some of the formulations discussed below are more easily adaptable for describing the kinetics of geothermometry. However, the generalized form of the expression above is very useful in particular for cases where diffusion is not the only kinetic process at play (e.g. diffusion + dissolution/precipitation).

**(ii) Kinetics of compositional preservation during cooling from a peak temperature for two mineral grains exchanging elements that are in contact with each other:** The formulation for this situation is due to Lasaga (1983) and related works. For a system cooling linearly from a peak temperature obeying  $T \approx T_p - s t$  where  $T$  is temperature,  $T_p$  the peak temperature,  $s$  the initial cooling rate and  $t$  is time, the partition

coefficient ( $K_D$ ) and diffusion coefficient are considered to decay exponentially with time obeying

$$K_D(t) = K_D^o e^{-\beta' t}$$

and

$$D(t) = D_o e^{-\gamma t}$$

The parameters controlling the variations,  $\beta'$  and  $\gamma$ , are given by

$$\beta' \equiv \frac{\Delta H^o s}{RT_p^2}$$

and

$$\gamma \equiv \frac{E s}{RT_p^2}$$

The role of the exchange partner of a crystal was described by a parameter,  $\beta/\gamma$ , where

$$\beta = \frac{\Delta H^o s \sqrt{D_B^o/D_A^o}}{RT_p^2 \{ \sqrt{D_B^o/D_A^o} [1 + (C_{1A}^l/C_{2A}^l)] + [(C_{1A}^l/C_{1B}^l) + (C_{1A}^l/C_{2B}^l)] \}}$$

which depends on the concentrations of various exchanging elements, the rate of diffusion in the two minerals, and most notably, the enthalpy change of the element exchange reaction,  $\Delta H^o$ .  $C_{1A}^l$  refers to the 'initial' composition of component 1 in mineral A; other  $C_{XX}^l$  terms may be interpreted analogously.

Using these quantities, ultimately the kinetics of compositional resetting in a given crystal, for a particular value of  $\beta/\gamma$ , is described by a parameter,  $\gamma'$ , given by equation 5:

$$r' = \frac{E s a^2}{R \cdot (T_p)^2 \cdot D_p} \quad (5)$$

where  $E$  is the activation energy,  $D_p$  is the diffusion coefficient at the peak temperature,  $T_p$ ,  $s$  is the cooling rate,  $a$  is a relevant length scale and  $R$  is the universal gas constant. Two values of  $\gamma'$  are particularly relevant (for a  $\beta/\gamma$  of 0.15 or so which is typical of many Fe-Mg exchange geothermometers) for  $\gamma' > 10$ , the composition at the peak temperature is preserved at the core of a crystal, and for  $\gamma' > 100$  most of the crystal retains its peak composition and only the very rims are reset. These provide important and useful guidance for the choice of systems and compositions for geothermometry, geospeedometry and geochronology. It is seen easily from equation 5 that different minerals (with

different values of relevant diffusion parameters e.g.  $E$ ,  $D_p$ ) in the same rock would preserve compositions to different extents, as would different grain sizes of the same mineral. It is interesting to note that aside from the role of the exchange medium, the expressions for  $\gamma'$  in the Lasaga formulations and  $T_c$  in the Dodson formulations depend on similar variables and in a similar manner. Even though the work was focused on garnets, Chakraborty and Ganguly (1991, their fig. 19) provided a discussion and an easy-to-use graphical representation of these relationships, that can be used to evaluate the extent of compositional resetting for any element exchange thermometer as long as  $\beta/\gamma$  lies close to 0.15.

**(iii, iv) Kinetics of element exchange mediated by a grain boundary:** If two grains are physically separated from each other, properties of the intervening matrix come into play as well in determining the extent of compositional readjustment. Early treatments of this effect include the fast grain boundary diffusion models of Eiler *et al.* (1992) and a similar treatment by Jenkin *et al.* (1994). As the name indicates, these models operate under the assumption that transport in the grain boundary for all elements is infinitely fast and effective. However, it has been shown, specifically for mantle minerals, that not all elements are incorporated in a grain boundary to the same extent (e.g. Hiraga *et al.*, 2003; Hiraga *et al.*, 2004). This phenomenon is well known in the materials science literature and is described by the grain-boundary segregation factor. Moreover, rates of grain boundary transport of different elements also differ by several orders of magnitude (e.g. see a review by Dohmen and Milke, 2010).

The role of these factors (i.e. concentration of an element in a grain boundary, its diffusion rate in the grain boundary, as well as the rate at which the element is exchanged between a crystal and the grain boundary) have been considered in a quantitative model by Dohmen and Chakraborty (2003). Implications for thermobarometry have been considered in that work as well as by Chakraborty and Dohmen (2001). The main finding was that the behaviour of such systems (two minerals exchanging elements/isotopes via an intervening medium) depend on three non-dimensional parameters ( $\beta$ ,  $\gamma$  and  $\delta$ ) that consist of: (1) diffusivity of the relevant elements/isotopes in the mineral grains; (2) diffusivity of the same elements/isotopes in the grain boundary of the intervening medium; (3) solubility of the element/isotope in the grain boundary region ('segregation factor' in the Materials Science literature); (4) grain sizes of the grains; (5) surface area of the minerals (related to grain size); (6) surface exchange reaction rate; and (7) distance between the mineral grains, and surface area of the grain boundary network. Depending on the values of these various parameters, six different kinds of situations (rather than the classical 'diffusion-control' or 'interface-control') may obtain. These have been depicted in a reaction mechanism map by Dohmen and Chakraborty (2003) (Fig. 2, where the non-dimensional parameters  $\gamma$ ,  $\delta$  and  $\beta$  are defined as well). For many situations related to geothermobarometry in relatively coarse-grained high-temperature rocks (igneous rocks, metamorphic rocks, mantle samples), three of these domains, the 'solid-diffusion control' domain, the 'fluid diffusion-control' domain, and a mixture of the two, are relevant. A property of particular importance is the solubility of the element of interest in the intervening medium; this changes substantially in melt-

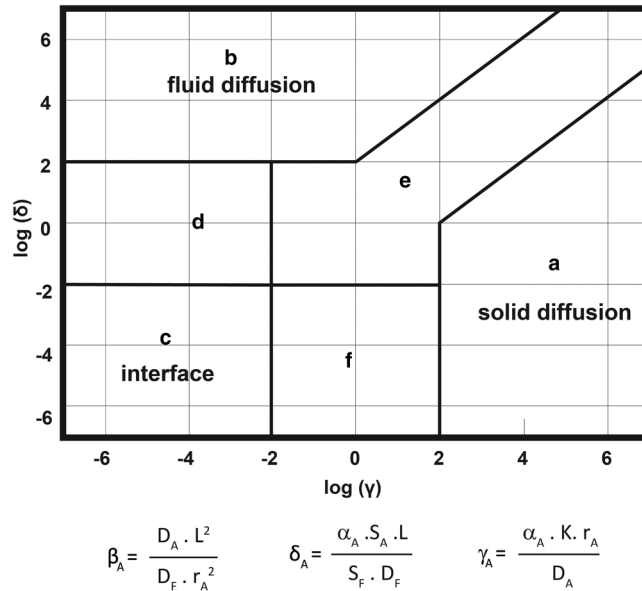


**Fig. 2.** Reaction mechanism map of Dohmen and Chakraborty (2003). Instead of a binary classification of kinetics into ‘diffusion control’ and ‘interface control’, for diffusive element exchange kinetics, we have several possible situations that are labeled a–f, depending on two non-dimensional parameters,  $\gamma_A$  and  $\delta_A$  while the rate depends on a third non-dimensional parameter,  $\beta_A$ .

The parameters are defined in the figure. Symbols used in the definition are:  $D_A$ : Diffusivity of the element in mineral grain A,  $D_F$ : Diffusivity of the element in the grain boundary ‘fluid’,  $L$ : distance along the grain boundary between the two grains,  $r_A$ : radius/half width of grain A,  $S_A$ : surface area of grain A,  $S_F$ : surface area along grain boundary between the two grains, A and B, that are exchanging the element,  $\alpha_A$ : kinetic constant for surface reaction for exchange of the element between mineral A and grain boundary ‘fluid’, and  $K$ : Partition coefficient of element in the grain boundary ‘fluid’, defined as  $K = (\text{Concentration in ‘fluid’}) / (\text{Concentration in solid A})$ . For details, see Dohmen and Chakraborty (2003).

The reaction mechanism map shows the different mechanisms that arise for different values of  $\gamma_A$  and  $\delta_A$ . (a) Classical diffusion control, with exchange controlled by diffusion rates in the solid. (b) Fluid diffusion control, where diffusion is controlled by the rate of transport (diffusion, solubility) in the grain boundary fluid medium. The ‘fluid’ can be physical (e.g. aqueous fluid, melt) or virtual (a dry grain boundary with its own transport properties). (c) Classical interface control where element exchange is controlled by the kinetic rate of exchange at the mineral–grain boundary interface. (d) Mixed interface–fluid diffusion control, which has characteristics of both (b) and (c), (e) a zone of mechanism that is a mixed control of solid and fluid diffusion control, or even all three end-member mechanisms: solid-, fluid- and interface-diffusion control, (f) a mixed zone of solid diffusion and interface control. The behaviour of crystals are different in each of these cases, and must be evaluated on a case-by-case basis to decide which compositions may be suitable for geothermometry. In several cases (e.g. fields (b), (d) or (c) even the rims of two crystals are not always in equilibrium with each other; in other cases the rims may be in equilibrium, but not the cores (depending on the value of the third parameter, the rate  $\beta_A$ ).

present vs. melt-absent situations. The presence of melt facilitates attainment of equilibrium between at least the rims of two grains that are physically separated from each other.

Based on all of these considerations, there are a few criteria that may be used to determine whether compositions of two such grains are suitable for geothermobarometry. If the rim compositions of all grains of a mineral, irrespective of distance from the exchange partners, are the same then there is a high likelihood that the composition is in equilibrium. If this applies to both elements involved in an exchange process, then it is possible that the core compositions of the two minerals may be paired to obtain the temperature/pressure at an earlier stage of evolution (see above for the parameter  $\gamma'$  that provides guidance in this matter). In addition, of course, chemical criteria that have been mentioned above (e.g. Roozeboom diagram), need to be tested. This highlights the importance of compositional measurements in a textural context, with attention to initial and boundary conditions under which the element/isotope exchange process occurred, rather than in isolated grains. For example, as seen from the above discussion, distance between the grains exchanging the element may be relevant, depending on the mechanism of reaction that operated. This requirement relates to single-mineral thermobarometry as well, where the 'single mineral' aspect arises from certain assumptions about the nature of the exchange partner/medium (e.g. fixed activity of certain components). Dohmen and Chakraborty (2003) demonstrated how it is possible to get artefacts and even temperatures higher than any that were ever attained if these criteria are not properly applied.

The overall outcome of the above analysis is that a simple analysis of diffusion using a  $x^2 \sim Dt$  kind of framework, or a simple calculation of closure temperature using the conventional textbook expression of the Dodson equation, is inadequate for evaluating which thermometers are reset to what extents, or even what the temperature given by a given thermometer means. We note, however, that the general expressions of Dodson (1973) or its later extensions (e.g. Ganguly and Tirone, 1999), used judiciously do permit such evaluations.

Before considering the specific natural system of interest, we summarize below a few lessons/corollaries that follow from the mathematical formulations of the kinetics of element exchange that have been described above:

### **Lesson 1: Multiple processes in series or parallel; the special status of diffusion + growth/dissolution**

As rocks are subjected to changing conditions (change in pressure or temperature, change in oxygen or water fugacity due to hydration/dehydration, or due to melt-rock interaction, as discussed in the example below) minerals adjust their compositions by a combination of diffusion processes and growth/dissolution of existing crystals (Fig. 3). As illustrated in Fig. 3, dissolution/precipitation can reduce/increase the size of a crystal, but compositional changes must involve diffusion (defined as the relative motion of a particle relative to another particle) in the fluid as well as the solid. As these processes with rather different kinetic rates occur together, expressions that consider the kinetics of processes occurring in series (i.e. sequentially after one after the other) or in parallel need to be considered. For processes that occur in parallel, the fastest sub-process is rate controlling; for processes that occur in series, it is the

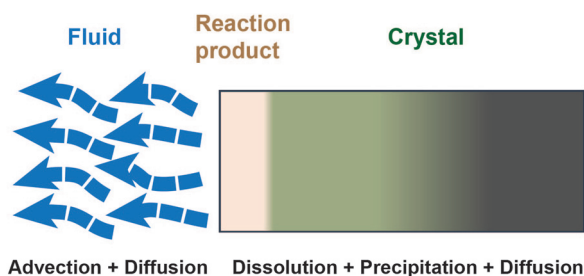


**Fig. 3.** Schematic depiction of a dissolution–precipitation reaction involving a mineral solid-solution. The process of dissolution and precipitation is, by itself, only a removal/addition of crystalline material. For a solid solution, the reactivity (solubility/saturation limit in the fluid) is invariably different for the different components of the solid solution. This leads to the production of concentration gradients in the crystal, with resulting diffusion (shown by colour gradation), and in the fluid where advection of the fluid and diffusion in the fluid act together.

slowest one. Therefore, in spite of the occurrence of dissolution/precipitation, diffusion rates continue to play a central role in the overall evolution. See fig. 2 and the discussion of the Dohmen and Chakraborty (2003) model above for examples of how diffusion in the solid as well as the fluid phases may be coupled and play a role in the overall exchange process. It is worthwhile noting, in the context of application of the generalized Dodson equation (equation 1), that in many cases the process of dissolution/precipitation + diffusion may be described by an effective diffusion equation and the process even depends on the same parameter,  $\delta$ , that has been described above in the Dohmen and Chakraborty formulation (see Lasaga, 1986, 2014 for derivations and discussion).

There are important implications of this for thermobarometry. During diffusive exchange, the core composition of a crystal may retain the ‘memory’ of a previous stage, the rim composition relates to a later stage in the evolution of the rock (e.g. dependent on the values of the parameters  $\beta/\gamma$  and  $\gamma'$  discussed above). But if adjustment of composition occurs by growth-dissolution where grains may recrystallize completely, this is not the case and the composition at the core may reflect the point in time when the dissolution/precipitation process occurred. The challenge lies in the fact that in real systems it is rarely an either/or situation; more commonly the two processes occur in conjunction. The first outcome is that one may have compositionally zoned minerals, bearing signatures of diffusion, but for thermobarometry (as well as geospeedometry/diffusion chronometry) one needs to decide, which, if any, compositions of other minerals may be paired with compositions in the zoned mineral for thermobarometry. Second, depending on the relative rates of growth/dissolution vs. diffusion, one may obtain homogeneous grains which are not in equilibrium with each other (see Dohmen and Chakraborty, 2003, for examples). Therefore, it is important to carry out chemical tests for (local) equilibrium (including the Roozeboom diagrams mentioned above) before calculating temperatures and pressures rather than rely on compositional zoning or homogeneity (see example below).

**Lesson 2: Lifetime of a crystal vs. lifetime of a phase; the role of textural maturation**

The important role of the textural context of compositional evolution leads to additional effects that arise from textural maturation. Even when a system is not chemically out of equilibrium, the need to minimize surface/interfacial free energy, and hence surface area of minerals, can drive grain growth and dissolution. A well-known example of such a process is Ostwald ripening; an outcome of this aspect is that existing grains (e.g. finer-grained ones) may dissolve to permit growth of other (e.g. coarser) grains. There may be other situations as well. Two common processes of particular relevance to the study of mantle samples are the following: (1) permeation of externally derived melt through a matrix may facilitate textural maturation and compaction processes, leading to dissolution of existing grains/parts of grains and precipitation of new material (with modified compositions); and (2) plastic deformation involves the motion of dislocations and this may lead to the annihilation of existing old grains the birth of new grains with new compositions (e.g. Hackl and Renner, 2013).

These have important consequences for geothermobarometry (and geochronology, geospeedometry) in that: (1) the evolution of compositional zoning in minerals, (2) the stage of evolution of a rock that is preserved in the compositional record of a mineral (= the last stage after such textural maturation process) are affected. Examples of how this may influence geological inferences from such data were provided by Beyer and Chakraborty (2021).

**Lesson 3: Multiple diffusion mechanisms, particularly of trace elements, and impact on closure temperatures**

It is being found increasingly that the diffusion of trace elements in minerals occurs by more than one mechanism, and hence rate, depending on their concentrations and other factors (e.g. oxygen fugacity, concentration in the surrounding medium). This effect was first shown for diffusion of Li in olivine (Dohmen *et al.*, 2010) and since recorded for many systems such as REE in olivine (Dohmen *et al.*, 2016), Al in olivine (Zhukova *et al.*, 2017), Li in zircon (Cisneros de León and Schmitt, 2019; Tang *et al.*, 2017), REE in garnet (Bloch *et al.*, 2020) and Nb, Ta, Hf, Zr in rutile (Dohmen *et al.*, 2019). In addition, major elements may occur in multiple sites in different minerals (such as Ca in garnets as grossularite or andradite components, Al in IV and VI coordination in several ferromagnesian minerals) and may therefore diffuse by different mechanisms (with different activation energies and other parameters of diffusion, see above for their role in kinetics). These lead to two consequences: (1) closure temperatures for different mechanisms may be different, and (2) either multicomponent coupling (e.g. Borinski *et al.*, 2012) or a reaction-diffusion equation involving homogeneous reaction between different “species” (= an element in different sites/part of different components, e.g. Dohmen and Chakraborty, 2010) is necessary to model the freezing behaviour accurately. Simplifications are possible, but the assumptions made in such simplifications

should be borne in mind. The implication for geothermobarometry is that depending on which mechanism and rate was operative in a given case (= different pre-exponential factors and activation energies), quite different stages of evolution of a rock may be recorded by the same trace element composition of a mineral; the results need to be interpreted accordingly.

In the following section we report data from an ophiolite sequence in Tibet (Xigaze/Luqu Ophiolite) to illustrate that simply pairing mineral compositions from such rocks without attention to kinetic factors leads to a large, indiscriminate scatter of calculated temperatures that cannot be interpreted in any meaningful manner. However, consideration of the kinetic factors not only produces a very systematic and kinetically meaningful pattern; it provides important insights into the evolution of the sequence as a whole.

#### **4. A case study from mantle samples from Xigaze Ophiolite, Tibet**

Mantle rocks are a multiphase system typically consisting of the phases olivine, orthopyroxene, clinopyroxene and spinel/garnet in different proportions, connected to each other via a grain boundary network. In addition, a melt phase may be present at different stages of evolution of a rock. Commonly, mantle peridotites experience several events of melt percolation, and depending on the exact location (e.g. which grain boundaries/contacts between minerals), magnitude (e.g. extent of melt pockets) and duration of such events, different thermometers may be reset to different extents. Minerals in direct contact under mantle conditions would maintain elemental exchange equilibrium. However, this equilibrium could be disturbed by many factors in ophiolitic mantle rocks before or during the emplacement process. Therefore, identification of element exchange equilibria for elements of interest between the phases that are present, and determination of whether they are at equilibrium or disequilibrium are crucial for acquiring meaningful temperature data and to further understanding the mechanisms affecting the processes endured by the rocks.

As discussed above, geothermometry in such systems requires the simultaneous application of thermodynamics and kinetics to determine temperatures and evaluate their significance. Additionally, it is necessary to evaluate whether concentration profiles are suitable for the determination of cooling rates before applying tools of geospeedometry.

We begin by introducing the rock suites used in the present study, followed by justifying the choice of analytical points for the determination of temperatures and then presenting the results. As will be seen, different thermometers record different sets of temperatures, more or less consistent with expectations based on diffusion rates of elements in the minerals that are involved in a geothermometer. However, a detailed analysis of concentration profiles reveal that the resetting was not entirely by diffusive processes (i.e. dissolution/precipitation played a role also; see above), and caution needs to be exercised in extracting cooling rates from these data.

#### 4.1. Geological setting and samples used in this study

The Yarlung-Zangbo Suture zone (YZS), the eastern segment of the Indus-Yalung Zangbo Suture (IYS) from the Nanga Parbat syntaxis (NPS) to the Namcha Barwa syntaxis (NBS), is the youngest suture among four major well-defined sutures in the Tibetan Plateau (Fig. 4a) (Dewey and Bird, 1970; Gansser, 1977; Molnar and Tapponnier, 1975; Yin *et al.*, 1988). Geographically, it is divided into three segments: the western segment (from Kiogar to Saga), the central segment (from Sangsang to Dazhuqu) and the eastern segment (from Zedong to the very east) (Hébert *et al.*, 2012). It marks the collision zone between the Indian (Greater Indian block) and Eurasian (Lhasa block) plates, in the wake of the Neotethyan ocean closure lasting from late Cretaceous to early Tertiary (Fig. 4A') (Allégre *et al.*, 1984; Dai *et al.*, 2013; Hébert *et al.*, 2012; Yin and Harrison, 2000).

The Luqu ophiolite, also called Beimarang or Xigaze ophiolitic massif (Girardeau *et al.*, 1985; Huot *et al.*, 2002), covers an area of  $\sim 150 \text{ km}^2$  at an elevation ranging from 3800 to 5000 m. It is located in the central segment (from Sangsang in the west to Dazhuqu in the east) and is sandwiched by the Xigaze Group flysch to the north and the Upper Jurassic-Lower Cretaceous red radiolarite and Trias-Lias flysch in fault contact to the south (Fig. 4a, b).

At Luqu, a continuous ophiolitic section is preserved exhibiting the complete lithospheric sequence (Huot *et al.*, 2002; Nicolas *et al.*, 1981). In the upper mantle section of the ophiolite, based on the mineralogical, petrographic and field relation characteristics, the ultramafic massifs can be divided into three groups (Fig. 4b). Group A: ultramafic massifs mainly consisting of fresh harzburgites, dunites and pyroxenites. Group B: ultramafic massifs mainly consisting of serpentized harzburgites, dunites, pyroxenites and abundant mafic dykes. Group C: ultramafic massifs mainly consisting of serpentinites, highly serpentized Cpx-harzburgites and lherzolites at the base of the mantle section.

In this paper, the studied samples are mainly selected from fresh harzburgite and dunite in group A (and chosen specific fresh samples in group B) as they maximally retain the magmatic features eliminating the effects of secondary alteration such as serpentization.

#### 4.2. Petrography

The fresh ultramafic rocks (harzburgite and dunite) generally have coarse to porphyroclastic textures. The latter texture is marked by the inequigranular mineral grains and the development of smaller neoblasts of olivine, orthopyroxene, clinopyroxene and spinel between pyroxene or olivine porphyroclasts. Based on the petrographic study, minerals in the rocks can be classified into different types and generations.

##### 4.2.1. Fresh Dunite

The fresh dunite consists of olivine ( $\sim 99 \text{ vol.}\%$ ), spinel ( $\sim 0.5 \text{ vol.}\%$ ) and Cpx ( $\sim 0.5 \text{ vol.}\%$ ) and a minor amount of sulfide, e.g. pentlandite. No orthopyroxene occurs in the dunite.

Olivine can be subdivided into three types according to the crystal size and mineral assemblage: (1) fine-grained olivine ( $\sim 20\text{--}100 \mu\text{m}$ ) occurs forming interstitial mineral

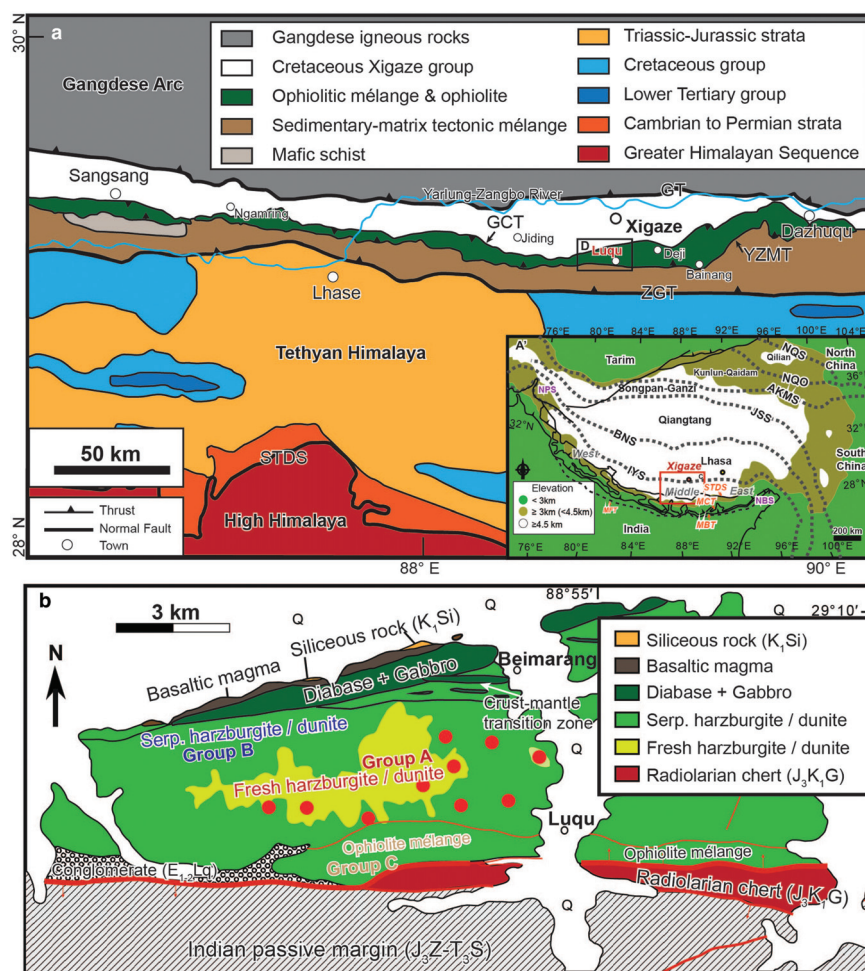


**Fig. 4.** (a) Geological map of the central segment of Yarlung-Zangbo Suture Zone (modified after Bédard *et al.*, 2009; Dai *et al.*, 2013; Ding *et al.*, 2005). Abbreviations: STDS, south Tibetan detachment system; ZGT, Zhongba-Gyangze thrust; YZMT, Yarlung-Zangbo Mantle thrust; GCT, Greater counter thrust; GT, Gangdese thrust. (A') Tectonic framework of Tibetan Plateau (modified after DeCelles *et al.*, 2002; Yin and Harrison, 2000). Abbreviations: MFT, Main Frontal Thrust; MBT, Main Boundary Thrust; MCT, Main Central Thrust; STDS, South Tibetan Detachment System; IYS, Indus-Yalung Zangbo Suture; BNS, Banggong-Nujiang Suture; JSS, Jinsha Suture; AKMS, Anyimaqen-Kunlun-Muztagh Suture; NQO, North Qaidam Orogen; NQS, North Qilian Suture; NPS, Nanga Parbat syntaxis; NBS, Namcha Barwa syntaxis. (b) Geological sketch map of Luqu ophiolite in Xigaze ophiolites (modified after Girardeau *et al.*, 1985; Nicolas *et al.*, 1981; Zhang *et al.*, 2017).

aggregates (Cpx+spinel+olivine) between the former two types of olivine (Fig. 5a). All the symplectic minerals of the aggregates are anhedral in shape and show no undulose extinction. (2) Coarse-grained olivine as porphyroclastic crystals (~1–3 mm) show

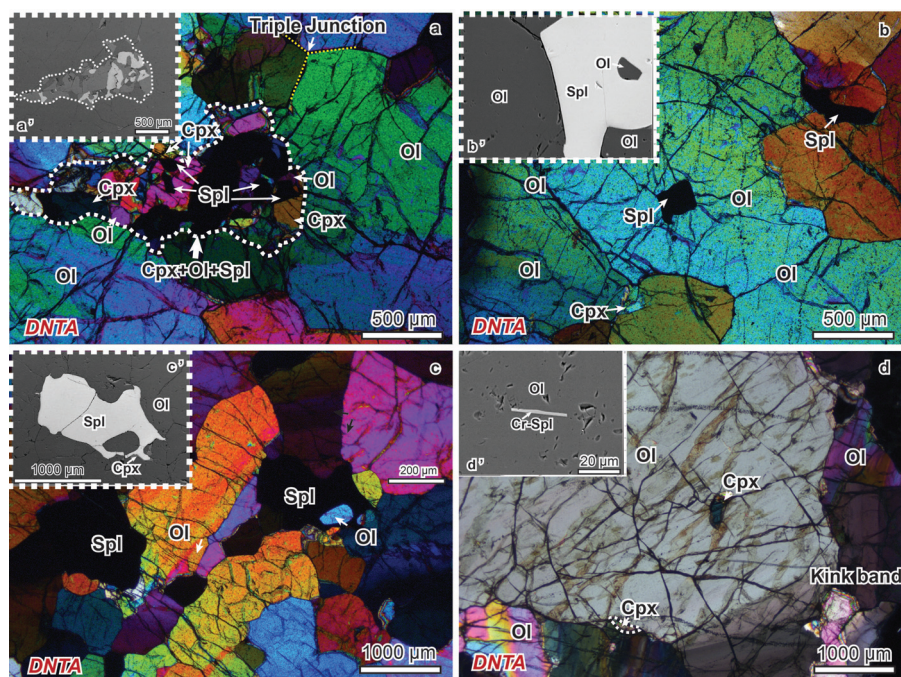


**Fig. 5.** Optical photomicrographs and (inset) backscattered electron images (BSE) of fresh dunite (Sample DNTA). The minerals are labelled in the individual frames, showing the different textural modes of occurrence of a mineral.

undulose extinction and kink bands. Some crystals host sparse inclusions of spinel and Cpx (Fig. 5b). (3) Medium- to coarse-grained olivine crystals ( $\sim 100\text{--}1000\ \mu\text{m}$ ) exist between the porphyroclastic ones. Triple junction texture is well-developed indicating recrystallization effects (Fig. 5c). Fewer amounts of mineral inclusions are observed in this type of olivine, but kink bands are common.

Spinel can be classified into the following types: (1) fine-grained crystals ( $\sim 30\text{--}100\ \mu\text{m}$ ) in anhedral shape occur in the interstitial mineral aggregate (Fig. 5a). (2) Fine-grained inclusions ( $\sim 30\text{--}100\ \mu\text{m}$ ) in olivine which are mostly euhedral (Fig. 5b). Occasionally, there are olivine inclusions in the spinel inclusion, and altogether enclosed in massive olivine (Fig. 5b). (3) Fine- to medium-grained anhedral crystals form an interstitial phase (Fig. 5b). (4) Medium-grained crystals ( $\sim 500\text{--}2000\ \mu\text{m}$ ) in subhedral to euhedral shape occur in the matrix of olivine (Fig. 5c). (5) Needle-shaped chromian spinel ( $\sim 30\ \mu\text{m}$  long) exists as inclusions in olivine (Fig. 5d).

Cpx generally occurs in the following four types. (1) Fine-grained crystals ( $\sim 30\text{--}100\ \mu\text{m}$ ) in anhedral shape occur in the interstitial mineral aggregates (Cpx + olivine + spinel) (Fig. 5a). (2) Fine-grained interstitial single crystals ( $\sim 100\ \mu\text{m}$ ) exist between olivine in subhedral to euhedral olivine (Fig. 5b). (3) Fine-grained interstitial crystal slices occur at the rim of medium-grained spinel (Fig. 5c). (4) Fine-

grained crystals ( $\sim 100\ \mu\text{m}$ ) in anhedral shape are included in the porphyroclastic olivine (Fig. 5d).

#### 4.2.2. Fresh Harzburgite

Olivine in the Cpx-bearing harzburgites is divided into five types. (1) Porphyroclastic olivine ( $\sim 500\text{--}5000\ \mu\text{m}$ ) contains euhedral spinel inclusions and are surrounded by fine- to medium-grained olivine, Cpx and spinel. Textures of kink and undulose extinction are well developed in the coarse-grained olivine type (Fig. 6a, b). (2) Fine- to medium-grained inclusions in spinel or in assemblage with anhedral spinel (Fig. 6b). (3) Medium-grained euhedral crystals are included Cpx (Fig. 6c). (4) Fine- to medium-grained crystals generally in subhedral shape recrystallize between the porphyroclastic olivine and opx. Triple junctions are prevalent (Fig. 6d). (5) Fine-grained olivine neoblasts occur at the embayments of porphyroclastic Opx as a part of the interstitial polyphase aggregates (Ol+Cpx+Spl  $\pm$  Opx  $\pm$  Pn) (Fig. 6b, d).

Opx can be classified into three types according to petrographic features. (1) Porphyroclastic crystals ( $500\text{--}3000\ \mu\text{m}$ ) bearing Cpx exsolutions (anhedral) and spinel inclusions (subhedral to euhedral) may be surrounded by the interstitial polyphase aggregates (Fig. 6a, d). (2) Fine- to medium-grained crystals exist in the interstitial polyphase

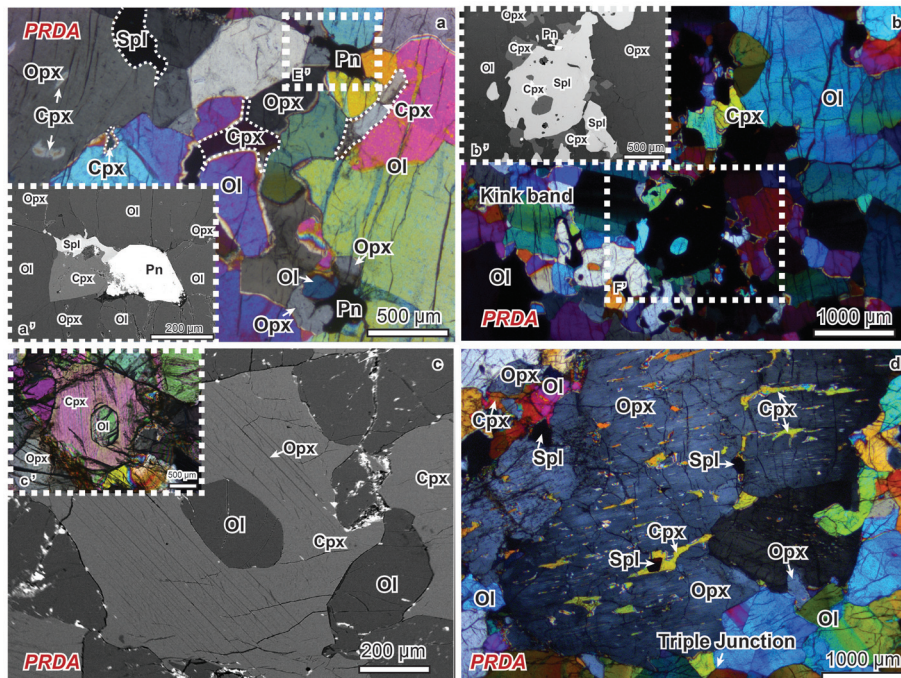


**Fig. 6.** Optical photomicrographs and (inset) backscattered electron images (BSE) of fresh harzburgite (Sample PRDA). Minerals are labelled in the individual frames, showing the different textural modes of occurrence of a mineral.

aggregate at the embayment of porphyroclastic opx (Fig. 6a, d). (3) Exsolution lamellae exsolved internally in medium-grained Cpx (Fig. 6c).

Cpx mainly occurs forming three types: (1) medium-sized crystals in subhedral shape, some of these crystals bear exsolution lamellae of Opx (thickness:  $\sim 1\text{--}2\ \mu\text{m}$ ) in their core (Fig. 6a, d). The width of Opx lamellae in Cpx is much thinner than the Cpx exsolution in Opx (thickness:  $\sim 3\text{--}10\ \mu\text{m}$ ) in the Opx porphyroclasts. (2) Fine-grained interstitial crystals in anhedral shape in the interstitial polyphase aggregate (Fig. 6b, d). (3) Fine-grained anhedral crystals in layered shape on the boundaries of spinel (Fig. 6b). (4) Cpx exsolution lamellae (thickness:  $\sim 3\text{--}10\ \mu\text{m}$ ) in the core of porphyroclastic Opx (Fig. 6a, b).

Spinel is identified as forming three types. (1) Fine-grained anhedral spinel occurs in interstitial polyphase aggregates ( $\text{Ol} + \text{Cpx} + \text{Spl} \pm \text{Opx} \pm \text{Pn}$ ) (Fig. 6a, b, c). (2) Medium- to coarse-grained subhedral to euhedral crystals occur between porphyroclastic olivine and Opx. Some spinel host inclusions of Cpx and Opx (Fig. 6b). (3) Fine-grained euhedral crystals as inclusions in porphyroclastic Opx (Fig. 6d).

The fine-grained interstitial phases are interpreted, based on their textural mode of occurrence as well as major- and trace-element (e.g. REE) compositional characteristics, to be products of crystallization from interstitial melt that must have percolated through the rock matrices.

### 4.3. Estimation of equilibrium temperatures

Compositional profiles across various mineral pairs in different textures were measured in an electron microprobe in the wavelength dispersive mode at Ruhr-Universität Bochum (Cameca SX Five-FE). Well established silicate and oxide standards were used with a  $1\ \mu\text{m}$  beam spot size and optimized step size. Data from such profiles, rather than isolated individual spot analyses, were used for evaluation of suitability for thermometry using the criteria discussed above.

As dunites and harzburgites in the Xigaze ophiolite that are studied here are both in the spinel-stable field, the pressure was set at 1.5 Gpa (15 Kbar) in all thermometric calculations for comparison. Mineral pairs were selected according to (a) the kinetic considerations outlined above, (b) bearing in mind the different textural modes of occurrence of a given mineral that has been described above, and (c) the nature of compositional zoning in the minerals. Next, the chemical analyses from such selected pairs are marked on the compositional profiles and projected on the Roozeboom diagram to show the compositional variation trends and test for approach to element partitioning equilibrium. Temperature ranges are reported only when mineral pairs pass these tests. It is seen that the same mineral pairs from different textural locations record different stages in the history of evolution of the rocks.

#### 4.3.1. Thermometry with spinel–olivine pairs as an example

The approximate linear ranges traversing the curves on the Roozeboom diagram indicate that compositions of each mineral pair are in equilibrium in such conditions (Fig. 7). Different temperatures (ranging from  $\sim 560$  to  $\sim 690^\circ\text{C}$ ) were estimated in different

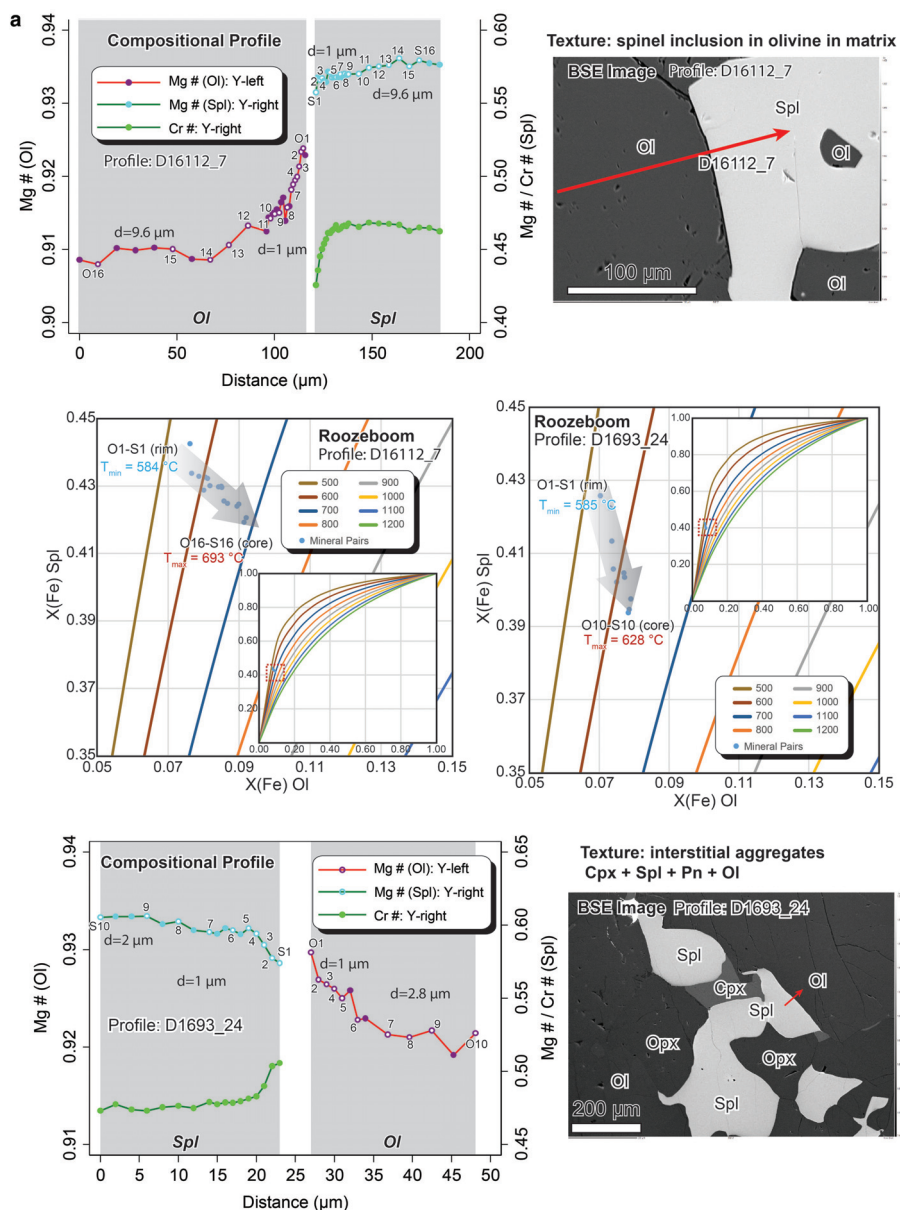


**Fig. 7.** Four selected compositional profiles across spinel–olivine for equilibrium temperature estimation. The BSE images show the location of the line measurements. Roozeboom diagrams indicate the equilibrium conditions among mineral pairs and the approximate temperature ranges. The  $T_{max}$  values at the core and  $T_{min}$  values at the interface are calculated using the thermometer of Ballhaus *et al.* (1991). Gaps indicate mixed analyses/cracks with alteration (i.e. not olivine/spinel stoichiometry) at interfaces. Images and profiles from fresh dunite (DNTA, sample 16112) and fresh harzburgite in group A (PRDA, Sample 1693).

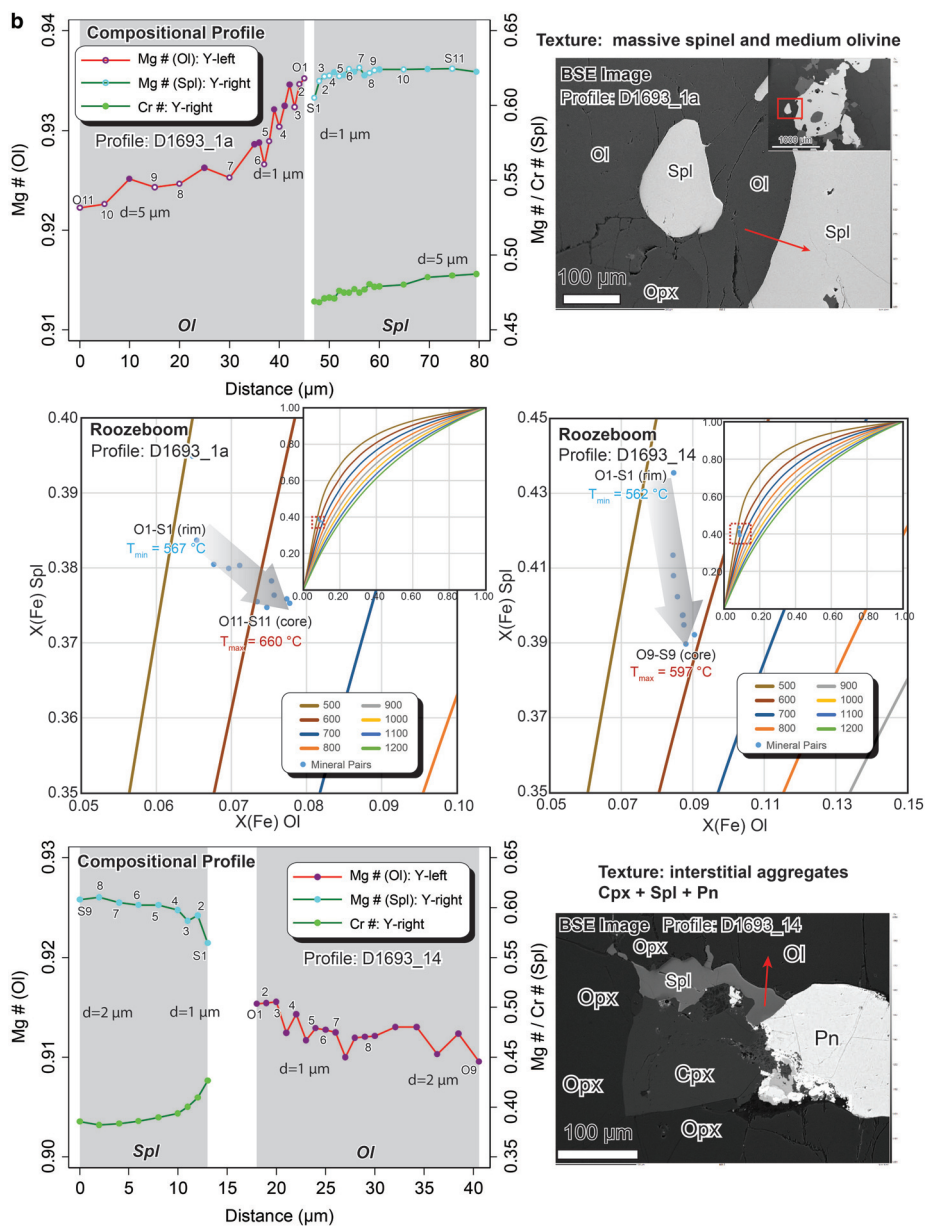


**Fig. 7b.** Continued.

spinel-olivine pairs among various textures (Table 1, Fig. 7). Analytical data points either from porphyroclastic olivine or massive spinel (larger grain size) record the higher  $T_{\text{max}}$  at the core part, and points from mineral pairs in the aggregates with smaller grain sizes

**Table 1.** Summary of the estimated temperatures (spinel–olivine) at the interface ( $T_{\min}$ ) and the core ( $T_{\max}$ ).

Profiles	D16112_7	D1693_24	D1693_1a	D1693_14
$T_{\max}$ (°C)	693	628	660	598
$T_{\min}$ (°C)	584	586	567	563
Texture	Ol: massive Spl: inclusion	Ol: interstitial Spl: interstitial	Ol: medium Spl: massive	Ol: interstitial Spl: interstitial

Profile D16112\_7: Fresh dunite in Group A (DNTA).

Profile D1693\_24, 1a & 14: Fresh harzburgite in Group A (PRDA1).

See Fig. 7 for more details.

record the lower  $T_{\max}$  (Fig. 7). On the other hand, temperatures ( $T_{\min}$ ) estimated at the interface of the mineral pairs are quite similar among occurrences in different textural modes. For example, spinel (massive)–olivine (medium) in profile D1693\_1a and spinel (inclusion)–olivine (massive) in profile 16112\_7 present  $T_{\max}$  values of 660°C and 693°C respectively. The  $T_{\max}$  values of the large grains are generally  $\sim 50^\circ\text{C}$  greater than that calculated from the mineral pairs in the polyphase aggregates. However, the temperatures at the interface ( $T_{\min}$ ) have a more minor variation (20°C) despite the various textures and mineral grain sizes. This overall distribution demonstrates clearly a history of progressive compositional resetting with resetting at rims at all textural locations > cores of smaller grains > cores of larger grains.

#### 4.3.2. Thermometry of spinel–orthopyroxene pairs

Two selected spinel and Opx pairs for equilibrium temperature estimates are listed below as examples (Fig. 8 & Table 2). The temperature estimated from the massive pairs with large grain size yield a higher  $T_{\max}$  (835°C) compared with the  $T_{\max}$  (783°C) from interstitial mineral pairs with very small grain sizes. Similar to the spinel–olivine pairs, the  $T_{\min}$  estimated from the rims of the two different scale gain sizes present only minor temperature differences (760°C in large grain sizes, 774°C in small grain sizes).

#### 4.3.3. Thermometry of clinopyroxene (Cpx)–orthopyroxene (Opx) pairs

The estimated temperatures among three different textures (massive, medium and exsolution) yield similar  $T_{\max}$  (890–904°C) using the analytical points obtained from near the mineral cores (Table 3, Fig. 9). The wide range of  $T_{\min}$  difference (768–893°C) might be caused by the loss of the measurement points bordering the interface of the mineral pairs (gradients at pyroxene–pyroxene interfaces are expected to be sharper than the others. This is partly a consequence of Fick’s law of diffusion: Flux = Diffusion coefficient  $\times$  concentration gradient. So, for smaller [slower] diffusion coefficients, as in pyroxenes, the gradients are steeper, making it more difficult to measure the exact rim compositions which may be in equilibrium with each other).

#### 4.3.4. Disequilibrium Mineral pairs

Equilibrium among different mineral pairs were not always attained in these ophiolite samples. Cpx–olivine pairs are a typical example of mineral pairs showing disequilibrium relationships. For example, the massive Cpx in the matrix is surrounded by medium-sized other phases, including olivine (Fig. 10). The equilibrium condition was tested by the

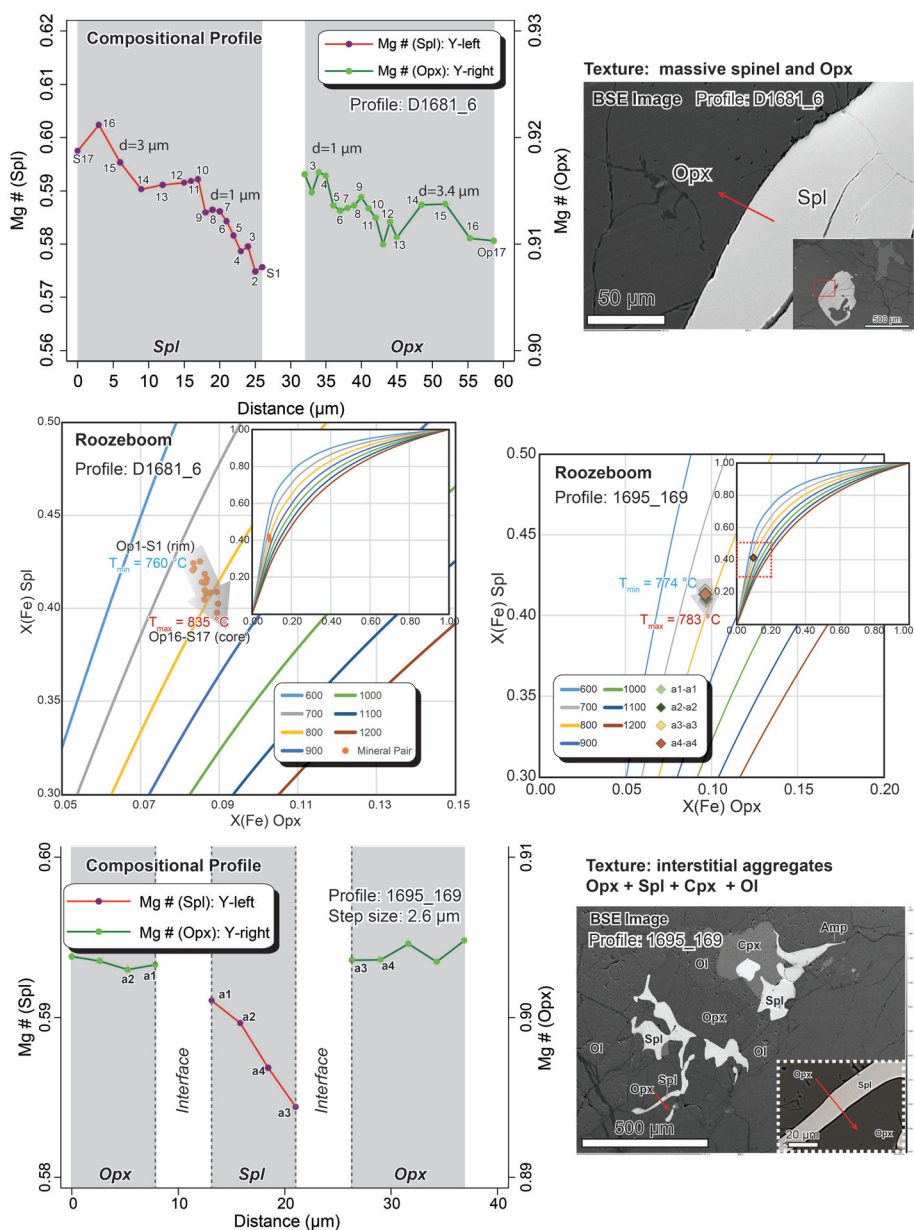


**Fig. 8.** Two selected compositional profiles across spinel–Opx pairs for equilibrium temperature estimation. The BSE images show the location of the line measurements. Roozeboom diagrams indicate the equilibrium conditions among mineral pairs and the approximate temperature ranges. The  $T_{\text{max}}$  values at the core and  $T_{\text{min}}$  values at the interface are calculated using the thermometer of Liermann and Ganguly (2003). Images and profiles from the harzburgite in group B (PRDB, Samples 1681 & 1695).

**Table 2.** Summary of the estimated temperatures (spinel–Opx) at the interface ( $T_{\min}$ ) and the core ( $T_{\max}$ ).

Profiles	1681_6	1695_169
$T_{\max}$ (°C)	835	783
$T_{\min}$ (°C)	760	774
Textures	Opx: massive Spl: massive	Opx: interstitial Spl: interstitial

Profile 1681\_16 & 1695\_169: Serpentinized harzburgite in Group B (PRDB1).  
See Fig. 8 for more details.

**Table 3.** Summary of the estimated temperatures (Cpx–Opx) close to the interface ( $T_{\min}$ ) and the core ( $T_{\max}$ ).

Profiles	16104c_273	16104_294	1681_14
$T_{\max}$ (°C)	901	890	904
$T_{\min}$ (°C)	893	782	768
Textures	Cpx: massive Opx: medium	Cpx: massive Opx: massive	Cpx: exsolution Opx: massive

Profile 16104c\_273 & 294: Fresh harzburgite in Group A (PRDA2).  
Profile 1681\_14: Serpentinized harzburgite in Group B (PRDB1).  
See Fig. 9 for more details.

mineral compositions in the Roozeboom diagram based on Kawasaki and Ito (1994). The compositional points are all projected above the curve of 1200°C in the Roozeboom diagram, indicating that equilibrium was not obtained in this case. Caution needs to be exercised when one estimates temperatures using such analytical data points from the Cpx–olivine pairs. If the test for equilibrium step is ignored, the estimated temperature, would be ~1300°C, which would be a meaningless number in this case.

#### 4.4. Concentration profiles and Diffusion modelling

Compositional zoning is used to obtain cooling rates using different techniques of geospeedometry. Often, compositional zoning in only one mineral is used, under the assumption that the composition at the core represents the composition at the peak temperature and then the retrograde zoning at the rim is modelled. From the discussion above it should be apparent that this condition is not fulfilled in many cases. Two pitfalls that arise commonly in many mantle (and other slowly cooled high-temperature rocks) are illustrated here through examples from the rocks studied here.

The first case in Fig. 11 demonstrates that the compositional profiles in adjoining mineral grains do not represent those due to an element exchange process. Element exchange would cause the concentration to decrease in one mineral and increase in the other. However, as seen in Fig. 11, the Mg# in both spinel and orthopyroxene increases towards the rim, indicating that there was an external source of the element (e.g. leakage/supply via the grain boundary between the two). Such supply may have occurred, for example, through a percolating melt phase. Clearly, the profiles are not suitable for modelling to obtain cooling/heating rates unless the boundary conditions for diffusion can be properly recognized and refined.

The second case in Fig. 12 shows a situation where the disposition of the profiles are in the right direction (i.e. gain in one, loss in the other), but a closer inspection reveals that

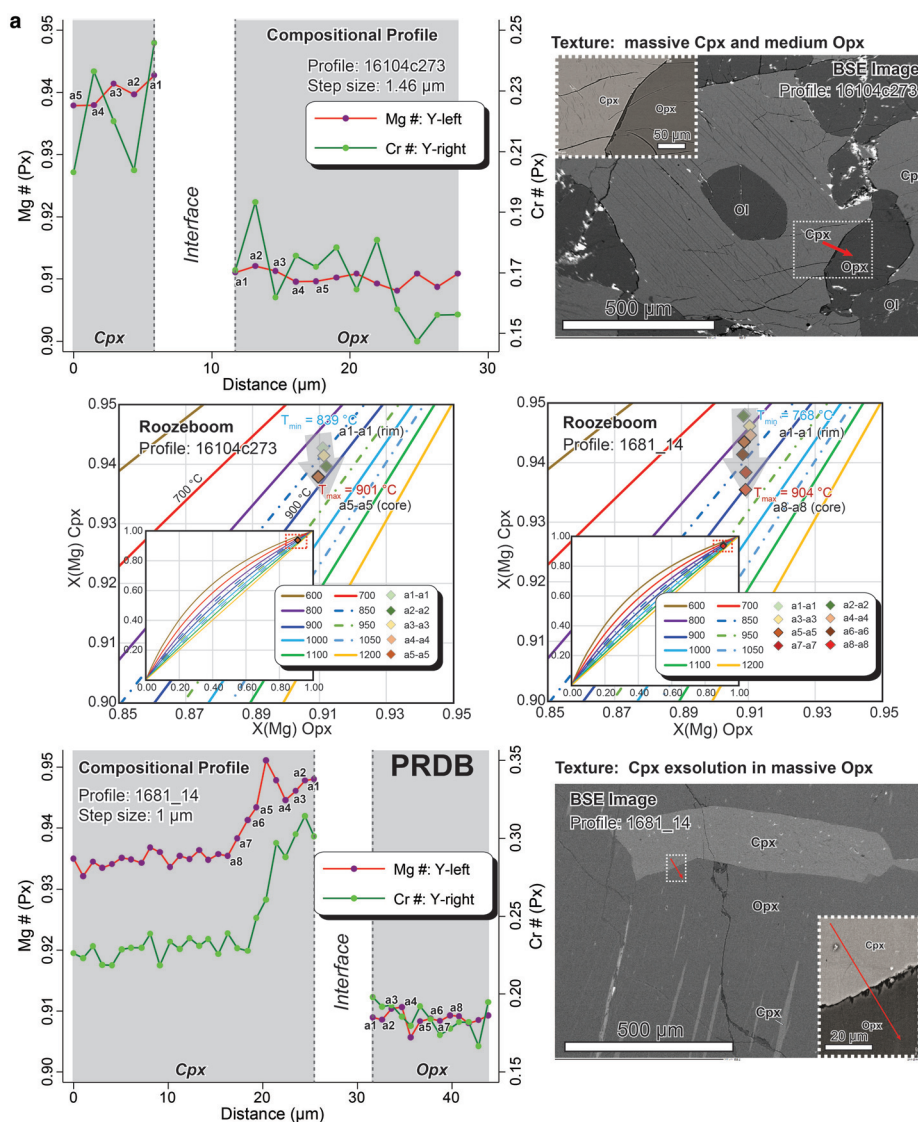


**Fig. 9.** Three selected compositional profiles across Cpx–Opx for equilibrium temperature estimation. The BSE images show the location of the line measurements. Roozeboom diagrams indicate the equilibrium conditions among mineral pairs and the approximate temperature ranges. The  $T_{\text{max}}$  at the core and  $T_{\text{min}}$  at the interface are calculated using the thermometer of Ganguly *et al.* (2013). Images and profiles from fresh harzburgite (DNTA, sample 16104) in group A and harzburgite (PRDB, Sample 1681) in group B.

the area under the two profile curves are not the same. This is a necessity for mass balance and diffusion modelling – the amount of element lost from one mineral (given by the area under the profile curve) must be compensated exactly by the gain in the other mineral.

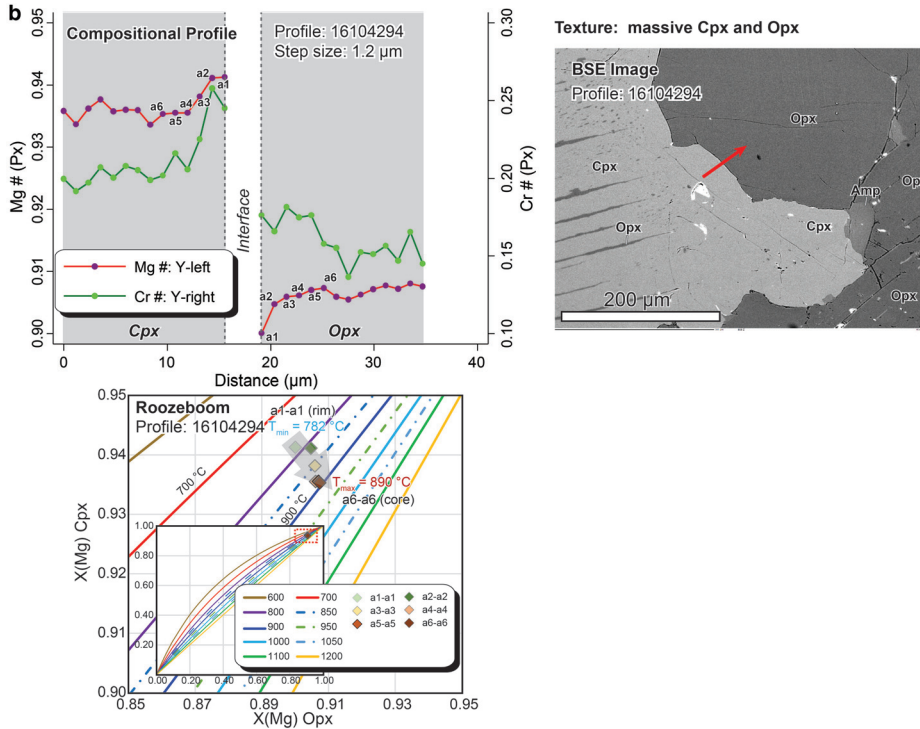


**Fig. 9b.** Continued.

Once again, even if the profiles show the right trends these are not suitable for modelling to obtain cooling/heating rates.

Both situations point to the operation of processes other than just element exchange by diffusion in these rocks. The petrographic and textural data reported above, that point clearly to the effects of melt percolation/infiltration and formation of multiple generations of minerals, provide an indication of possible processes that may have occurred: dissolution, precipitation and textural maturation (see lessons 1–3 above). On the whole, these underscore the need for evaluating the kinetic processes involved and the boundary conditions before applying diffusion models to determine cooling/heating rates; not all concentration profiles that have the appearance of diffusion profiles are amenable to diffusion modelling. Note that the shapes of the profiles themselves may be fit by diffusion models if single minerals are used; it is just that the cooling/heating rates that would be obtained would lack physical significance in these cases.

#### 4.5. Putting it together: implications for cooling history

Figure 13a summarizes the results of geothermometry carried out using: (a) all the different systems where equilibrium conditions were fulfilled (*REE* between Cpx-Opx

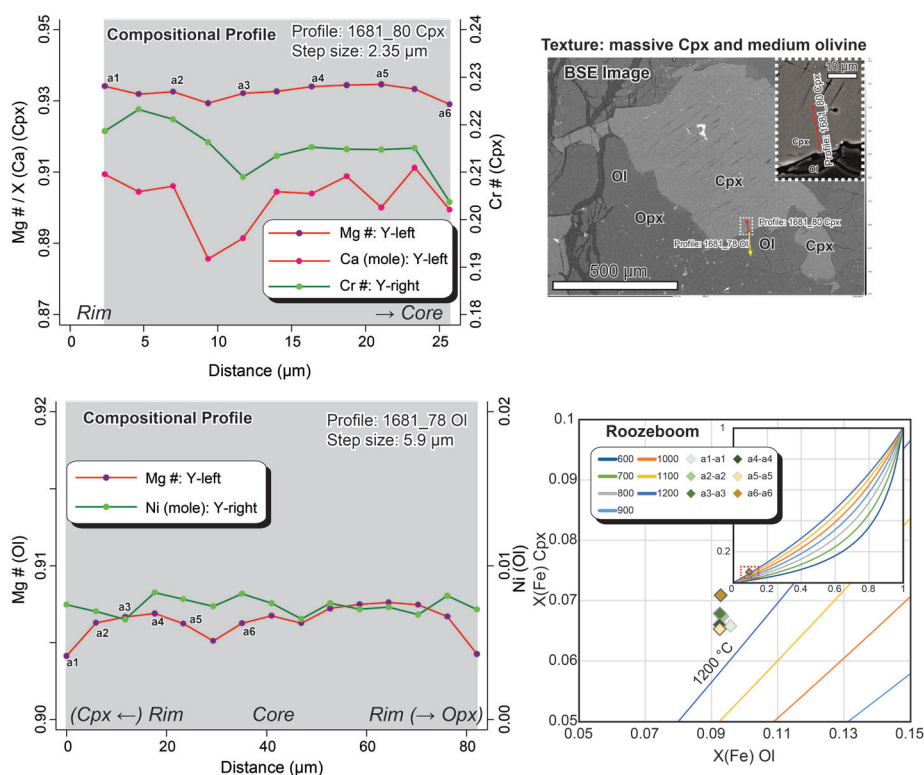


**Fig. 10.** One selected compositional profile across Cpx–olivine for equilibrium temperature estimation from harzburgite in group B (PRDB, sample 1681). The BSE image shows the location of the line measurement. The Roozeboom diagram indicates the equilibrium conditions among mineral pairs and the approximate temperature ranges (Kawasaki and Ito, 1994). The analytical points plot clearly outside the limits permitted by equilibrium at reasonable temperatures, indicating disequilibrium.

and Fe-Mg exchange between Opx-Cpx, Opx-spinel and Olivine-spinel) for (b) minerals occurring in the different textural modes in (c) all the different rock types. One observes several regularities in the pattern of the data.

First, temperatures from the same mineral pair from different rocks lie in the same range, emphasizing the kinetic control. Here, the usefulness of an ophiolite sequence compared to isolated mantle xenoliths becomes obvious; the spatial context provided by the field relations require that the different lithologies have gone through similar thermal histories (so that the same mineral pair should not yield widely different temperatures in these different rocks). At the same time, the different lithologies help to restrict/eliminate variabilities that may arise from bulk compositional control on the thermometers. The similarity of temperature obtained from different lithologies demonstrate that these, and the cooling histories, relate to the ophiolite sequence as a whole and not just to a particular rock type or outcrop.

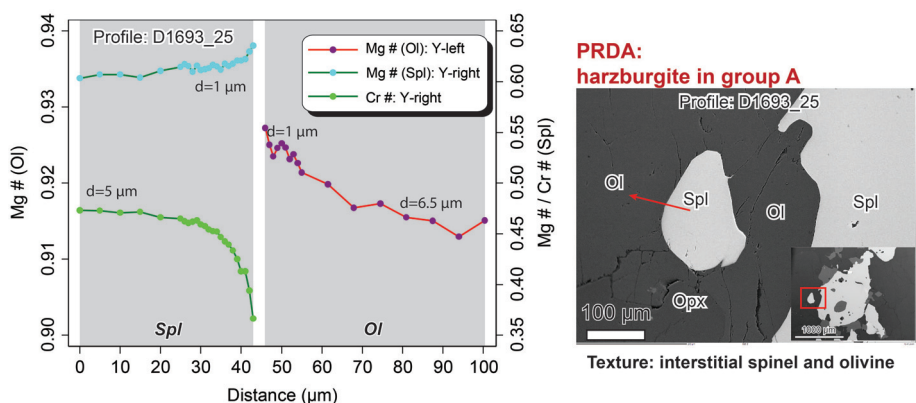


**Fig. 11.** Compositional profiles from an olivine–spinel contact (red line on the BSE image) that looks apparently clean but the profiles (left panel) do not correspond to shapes expected by element exchange between the two grains alone (Mg# increases towards the rim in both minerals). The sample is harzburgite PRDA in group A, sample number 1693.

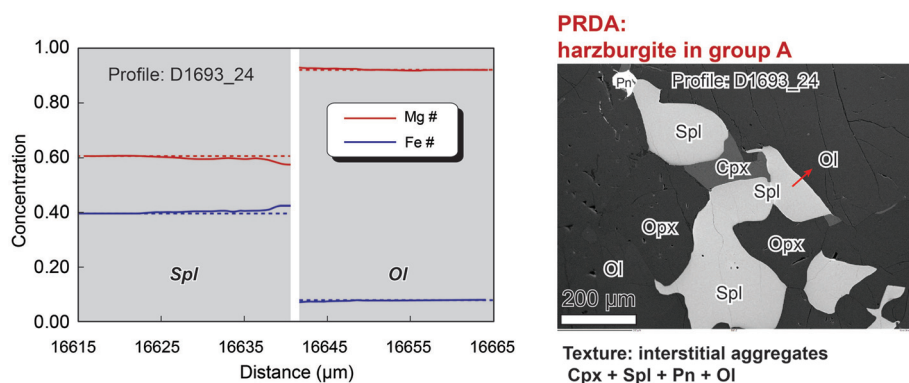


**Fig. 12.** Compositional profiles at an olivine–spinel contact (left panel) from a location shown by the red line in the BSE image (right panel). The areas under the profile curves show that mass balance is not obtained, and element exchange must have occurred between more partners than the adjacent olivine and spinel grains. This situation is unsuitable for geospeedometry modelling. The sample is harzburgite PRDA in group A, sample number 1693.

Second, the temperatures are sorted in the sequence expected from the diffusion parameters of the slower diffusing mineral in a pair (Table 4). Thus, REE from the two pyroxenes freeze at the highest temperature (1050–1250°C), followed by Fe–Mg in pyroxenes (750–1050°C), the spinel–orthopyroxene pairs (750–850°C), and the olivine–spinel pair was reset until freezing at the lowest temperatures below 750°C (600–750°C). Moreover, for a given mineral pair (e.g. olivine–spinel) and textural setting (e.g. matrix minerals) it is found that coarser spinel sizes yield greater temperatures compared to finer spinel grains

**Table 4.** Summary of the estimated temperatures using different thermometers among different coexisting mineral pairs.

ID	Sample ID	Profile ID	Label	Pairs	Grain Size	$T_{\min}$	$T_{\max}$	Texture
1	16112	16112_23	DNTA	Spl-Ol	50	620.10	683.37	3
2	16112	16112_73	DNTA	Spl-Ol	200	632.10	648.67	3
3	16112	16112_74	DNTA	Spl-Ol	200	614.60	646.60	3
4	16112	16112_22	DNTA	Spl-Ol	50	663.32	689.86	1
5	16112	16112_76	DNTA	Spl-Ol	80	680.63	695.22	1
6	16112	16112_72	DNTA	Spl-Ol	1000	677.10	748.97	0
7	16112	16112_9	DNTA	Spl-Ol	1500	714.03	742.93	0
8	16562	16562_1	PRDA2	Spl-Ol	200	659.90	679.29	1
9	1693	1693_2	PRDA1	Spl-Ol	800	685.44	688.59	1
10	1693	1693_2	PRDA1	Spl-Opx		828.00	846.00	1
11	16562c	16562_1	PRDA2	Spl-Opx		777.79	782.20	1
12	1695	1695_169	PRDB1	Spl-Opx		772.79	783.59	1
13	1681	1681_85	PRDB1	Spl-Opx		802.04	820.77	0
14	1681	1681_18	PRDB1	Spl-Opx		791.89	805.35	0
15	1693	1693_2	PRDA1	Cpx-Opx		903.73	924.25	2
16	1693	1693_266	PRDA1	Cpx-Opx		888.26	905.58	2
17	16562c	16562_154	PRDA2	Cpx-Opx		806.38	860.70	2
18	1693	1693_2	PRDA1	Cpx-Opx		946.36	991.05	1
19	16562c	16562_1	PRDA2	Cpx-Opx		901.46	959.35	1
20	16104c	16104_273	PRDA2	Cpx-Opx		839.24	900.69	0
21	1681	1681_18	PRDB1	Cpx-Opx		902.66	993.27	0
22	1681	1681_4	PRDB1	Cpx-Opx		909.25	1053.56	3
23	1681	1681_14	PRDB1	Cpx-Opx		768.97	903.93	3
24	16104v	16104v294	PXA1	Cpx-Opx		782.73	891.51	0
25	1317	1317_36	PXA2	Cpx-Opx		792.79	842.84	0
26	1317	1317_38	PXA2	Cpx-Opx		878.72	916.72	3
27	16562v	16562v80	PXA3	Cpx-Opx		859.49	912.60	0
28	16562v	16562v81	PXA3	Cpx-Opx		892.88	962.50	0
29	1693	1693_20	PRDA1	REE_2Px		1198.00	1240.00	2
30	1682v	1682v37	PXA3	REE_2Px		1022.00	1068.00	0
31	1695	1695_05	PRDB1	REE_2Px		1087.00	1151.00	0
32	1695	1695_03	PRDB1	REE_2Px		1106.00	1256.00	0
33	1681	1681_23	PRDB1	REE_2Px		1051.00	1073.00	2
34	1681	1681_24	PRDB1	REE_2Px			1075.00	2
35	16111	16111_11	PRDC	REE_2Px		1088.00	1118.00	0
0	Matrix							
1	Aggregate							
2	Exsolution							
3	Inclusion							

DNTA: Fresh dunite in Group A.

PRDA1: Fresh harzburgite in Group A (Mode (Cpx) &gt;3 vol. wt.%).

PRDA2: Fresh harzburgite in Group A (Mode (Cpx) &lt;3 vol. wt.%).

DNTB: Serpentinized dunite in Group B.

PRDB1: Serpentinized harzburgite in Group B (Mode (Cpx) &gt;3 vol. wt.%).

PRDB2: Serpentinized harzburgite in Group B (Mode (Cpx) &lt;3 vol. wt.%).

PRDC: Serpentinized Cpx-bearing harzburgite in Group C.

PXA1: Clinopyroxenite in Group A.

PXA2: Websterite in Group A.

PXA3: Orthopyroxenite in Group A.

PXB1: Orthopyroxenite in Group B.

(temperatures obtained from interstitial spinel grains fall totally outside of the trend, emphasizing the role of textural location and hence, reaction history; it is not just the grain size that controls the variability). This pattern highlights the important role of

diffusion in the freezing process, even if it has been clearly demonstrated that other processes such as dissolution, precipitation and textural maturation also played a role (such as through interaction with percolating melt; see the previous section).

This aspect may be seen more quantitatively by considering the non-dimensional parameters in the various models that were introduced earlier. In the context of the reaction mechanism map of Dohmen and Chakraborty (2003), the parameter  $\log \delta$  is  $\sim 9.0$  and  $\log \gamma > 13.0$  for all combinations of diffusion coefficients, grain sizes and other geometric parameters (e.g. distance between grains, surface area calculated based on average grain size; the surface reaction rate,  $\alpha$ , has been considered to be 1.0 in the absence of any available experimental data). This implies that the kinetics of element exchange in the samples were controlled essentially by a 'solid-diffusion control' mechanism; in some cases, a 'mixed solid-fluid diffusion control' may have operated, consistent with the inference in the previous paragraph. Given such 'solid diffusion control', the  $\gamma'$  parameter of Lasaga (1983) may be used to estimate approximately the freezing temperature range of different minerals. The calculation is approximate because: (a) the temperature depends on the exchange partner as well, and any given mineral in the sample (e.g. olivine) exchanged Fe and Mg with several other minerals (e.g. orthopyroxene, clinopyroxene, spinel), and (b) the mathematical analysis is based on a linear cooling history. In a thermally evolving rock system, for values of  $\gamma' < 10$ , even the composition at the core is reset while for  $\gamma' > 100$ , even the rim compositions remain frozen (Section 2.ii above). Thus, the range of temperatures obtained from the core and the rim compositions correspond roughly to the range  $10 > \gamma' > 100$ . This is illustrated in Fig. 13a, b. Figure 13b illustrates schematically how the different temperatures might relate to the overall thermal evolution of the rock package. The purple line in the figure, including pulses at the higher temperature partly resulting from melt percolation events, shows a possible thermal history followed by the ophiolite sequence. There is an overall continuous (but not necessarily constant) cooling trend. Superposed on this trend, the ranges of temperatures obtained from different geothermometers, which are expected to freeze at different temperatures based on the above considerations, are shown as different coloured bands (the ranges are the same in Figs 13a and 13b, and are based on measurements). It is seen that there is some overlap between freezing ranges of different thermometers (depending, for example, on the grain sizes of minerals used). Diffusion modelling can yield cooling rates from zoning profiles between cores and rims of crystals – this is illustrated through red arrows for spinel-orthopyroxene and spinel-olivine pairs. The depiction underscores that concentration profiles in different mineral pairs would potentially record cooling rates at different segments of the overall thermal history, and that these need not be the same – a mineral grain has no memory of temperatures where  $\gamma' < 10$ , and is not affected by the thermal history once  $\gamma' > 100$ .

Third, as discussed above, processes such as growth and dissolution of crystals also operated (e.g. related to melt percolation) and element transport occurred along grain boundaries (external supply/leakage in mineral exchange pairs) so that it was not possible to carry out quantitative geospeedometry using the profiles reported here. Nevertheless, the systematic pattern of freezing of the thermometers point to a relatively slow, and more or less continuous cooling of the ophiolite sequence during emplacement (the

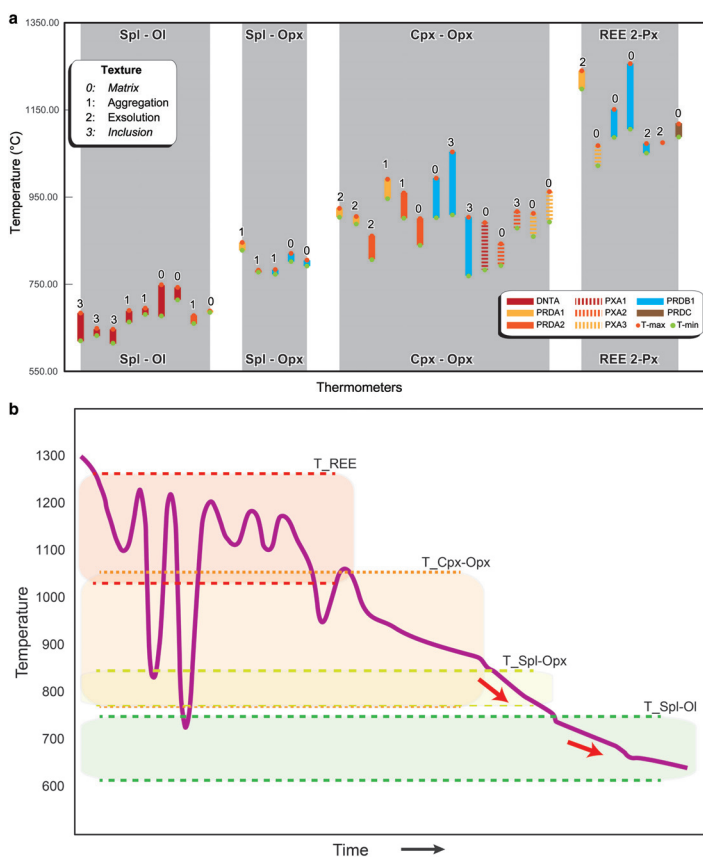


**Fig. 13.** (a) Summary of the estimated temperatures using different thermometers among different coexisting mineral pairs from different rocks (different colours) and different textural locations (numbers in legend). Temperatures obtained from different thermometers are different, but the behaviour is systematic across different rocks and mineral pairs, and are therefore physically meaningful. Please see text for more details and discussion of implications.

Mineral pairs in different colours are taken from DNTA: Dunite in Group A, PRDA1: Harzburgite in group A (Mode (Cpx) >3 vol. wt.%), PRDA2: Harzburgite in group A (Mode (Cpx) <3 vol. wt.%), PRDB1: Harzburgite in group B (Mode (Cpx) >3 vol. wt.%), PRDC: Cpx-bearing harzburgite in Group C, PXA1: Clinopyroxenite in group A, PXA2: Websterite in group A, PXA3: Orthopyroxenite in group A respectively.

(b) A schematic depiction of a possible thermal history for the ophiolite package (purple line) with the various temperature ranges recorded by different thermometers (various colours) in different textural settings (grain size, location of chemical analysis such as core or rim of a crystal as well as inclusion or matrix phase). The ranges recorded by a given thermometer are indicated by dashed lines of the same colour. Oscillations at high temperatures indicate the effect of melt percolation events. Temperatures may drop to quite low values between events, but the thermometers would be reset in successive events. And they freeze when the freezing temperature range is crossed finally (see text for details of kinetic parameters that control this). Red arrows indicate the segment of cooling history that may be accessed by diffusion modelling of compositional zoning in a given mineral pair, if suitable boundary conditions are fulfilled (see text for details). Note that these ranges are different for different mineral pairs, and that the cooling rates need not be the same over different segments of the thermal history.

different thermometers would freeze at similar temperatures for fast cooling, and the systematic pattern would not be present if cooling were not to be smooth). Note that this excludes neither changes in cooling rates at different temperatures, nor short thermal pulses (such as those that might be expected during a melt percolation event); see Fig. 13b. Indeed, the inability to describe all the compositions and compositional profiles in the different minerals (and in different textural locations, grain sizes) using simple diffusive exchange models, coupled with the petrographic observations of melt percolation and element exchange by processes other than pure diffusive-exchange between grains, underscore the role of coupled grain-scale melt transport, dissolution/precipitation, and diffusion processes.

## 5. Conclusions

We have outlined the importance of kinetics, and thereby chemical analysis with spatial-textural context, for performing geothermobarometry in mantle rocks. Some common formulations for kinetic treatment of element exchange thermometry, along with their implications for the practice of thermometry, have been summarized. We have illustrated the role of kinetics through applications to a suite of rocks from an ophiolite sequence (Xigaze ophiolite, Tibet). Taken together, the petrographic observations and mineral-chemical data point to multiple stages in the evolution of the rocks in the ophiolite sequence. Mineral growth and dissolution occurred together with diffusion during this evolution and overall cooling and emplacement of the sequence. Thermometry and geospeedometry of such mantle samples require evaluation of various kinetic aspects related to these processes. However, once such factors are considered, a very systematic pattern emerges pointing to a history of relatively slow and continuous cooling during emplacement of the ophiolite body.

## Acknowledgements

This research was supported financially by grants from the National Natural Science Foundation of China (41572044 and U1906207). Additional funds from the Ruhr Universität Bochum to SC helped fund the research. We acknowledge the help of the following through many discussions: Prof. Xuping Li, Dr Arne Willner, Dr Hans-Peter Schertl and Dr Ralf Dohmen.

## References

- Allégre, C.J., Courtillot, V., Tapponnier, P., Hirn, A., Mattauer, M., Coulon, C., Jaeger, J.J., Achache, J., Schärer, U., Marcoux, J., Burg, J.P., Girardeau, J., Armijo, R., Gariépy, C., Göpel, C., Li, Tindong, Xiao, Xuchang, Chang, Chenfa, Li, Guangqin, Lin, Baoyu, Teng, Jiwen, Wang, Naiwen, Chen, Guoming, Han, Tonglin, Wang, Xibin, Den, Wanming, Sheng, Huaibin, Cao, Yougong, Zhou, Ji, Qiu, Hongrong, Bao, Peisheng, Wang, Songchan, Wang, Bixiang, Zhou and Yaoxiu & Ronghua, Xu (1984) Structure and evolution of the Himalaya–Tibet orogenic belt. *Nature*, **307**(5946), 17–22.

- Ballhaus, C., Berry, R. and Green, D.H. (1991) High pressure experimental calibration of the olivine–orthopyroxene–spinel oxygen geobarometer: implications for the oxidation state of the upper mantle. *Contributions to Mineralogy and Petrology*, **107**(1), 27–40.
- Bédard, É., Hébert, R., Guilmette, C., Lesage, G., Wang, C.S. and Dostal, J. (2009) Petrology and geochemistry of the Saga and Sangsang ophiolitic massifs, Yarlung Zangbo Suture Zone, Southern Tibet: Evidence for an arc–back-arc origin. *Lithos*, **113**(1), 48–67.
- Beyer, C. and Chakraborty, S. (2021) Internal stress-induced recrystallization and diffusive transport in CaTiO<sub>3</sub>–PbTiO<sub>3</sub> solid solutions: A new transport mechanism in geomaterials and its implications for thermobarometry, geochronology, and geospeedometry. *American Mineralogist*, **106**(12), 1940–1949.
- Bloch, E.M., Jollands, M.C., Devoir, A., Bouvier, A.-S., Ibañez-Mejía, I. and Baumgartner, L.P. (2020) Multi-species Diffusion of Yttrium, Rare Earth Elements and Hafnium in Garnet. *Journal of Petrology*, **61**(7), ega055.
- Borinski, S.A., Hoppe, U., Chakraborty, S., Ganguly, J. and Bhowmik, S.K. (2012) Multicomponent diffusion in garnets I: general theoretical considerations and experimental data for Fe–Mg systems. *Contributions to Mineralogy and Petrology*, **164**(4), 571–586.
- Chakraborty, S. and Dohmen, R. (2001) Some aspects of the role of intergranular fluids in the compositional evolution of metamorphic rocks. *Journal of Earth System Science*, **110**(4), 293–303.
- Chakraborty, S. and Ganguly, J. (1991) Compositional zoning and cation diffusion in garnets. Pp. 120–175 in: *Diffusion, Atomic Ordering, and Mass Transport*. (J. Ganguly, editor). Selected Topics in Geochemistry. Springer US, New York.
- Cisneros de León, A. and Schmitt, A.K. (2019) Reconciling Li and O diffusion in zircon with protracted magmatic crystal residence. *Contributions to Mineralogy and Petrology*, **174**(4), 28.
- Dai, J., Wang, C., Polat, A., Santosh, M., Li, Y. and Ge, Y. (2013) Rapid forearc spreading between 130 and 120 Ma: evidence from geochronology and geochemistry of the Xigaze ophiolite, southern Tibet. *Lithos*, **17**, 1–16.
- DeCelles, P.G., Robinson, D.M. and Zandt, G. (2002) Implications of shortening in the Himalayan fold-thrust belt for uplift of the Tibetan Plateau. *Tectonics*, **21**(6), 121–12-25.
- Dewey, J.F. and Bird, J.M. (1970) Mountain belts and the new global tectonics. *Journal of Geophysical Research*, (1896–1977), **75**(14), 2625–2647.
- Ding, L., Kapp, P. and Wan, X. (2005) Paleocene–Eocene record of ophiolite obduction and initial India-Asia collision, south central Tibet. *Tectonics*, **24**(3), 1–18.
- Dodson, M.H. (1973) Closure temperature in cooling geochronological and petrological systems. *Contributions to Mineralogy and Petrology*, **40**(3), 259–274.
- Dodson, M.H. (1976) Kinetic processes and thermal history of slowly cooling solids. *Nature*, **259**(5544), 551–553.
- Dodson, M.H. (1986) Closure Profiles in Cooling Systems. *Materials Science Forum*, **7**, 145–154.
- Dohmen, R. and Chakraborty, S. (2003) Mechanism and kinetics of element and isotopic exchange mediated by a fluid phase. *American Mineralogist*, **88**(8-9), 1251–1270.
- Dohmen, R. and Milke, R. (2010) Diffusion in Polycrystalline Materials: Grain Boundaries, Mathematical Models, and Experimental Data. *Reviews in Mineralogy and Geochemistry*, **72**(1), 921–970.
- Dohmen, R., Kasemann, S.A., Coogan, L. and Chakraborty, S. (2010) Diffusion of Li in olivine. Part I: Experimental observations and a multi species diffusion model. *Geochimica et Cosmochimica Acta*, **74**(1), 274–292.
- Dohmen, R., Marschall, H., Wiedenbeck, M., Polednia, J. and Chakraborty, S. (2016) Trace element diffusion in minerals: the role of multiple diffusion mechanisms operating simultaneously. AGU Fall Meeting Abstracts, pp. MR51A–2682.
- Dohmen, R., Marschall, H.R., Ludwig, T. and Polednia, J. (2019) Diffusion of Zr, Hf, Nb and Ta in rutile: effects of temperature, oxygen fugacity, and doping level, and relation to rutile point defect chemistry. *Physics and Chemistry of Minerals*, **46**(3), 311–332.
- Eiler, J.M., Baumgartner, L.P. and Valley, J.W. (1991) Numerical modeling of diffusive exchange of stable isotopes in the lithologic setting, Abstracts with Programs-Geological Society of America. Geological Society of America, pp. A447–A447.

- Eiler, J.M., Baumgartner, L.P. and Valley, J.W. (1992) Intercrystalline stable isotope diffusion: a fast grain boundary model. *Contributions to Mineralogy and Petrology*, **112**, 543–557.
- Ganguly, J. (2021) Academic Reminiscences and Thermodynamics–Kinetics of Thermo–Barometry–Chronology. *Geochemical Perspectives*, **10**(1), 1–3.
- Ganguly, J. and Saxena, S.K. (1987) Exchange equilibrium and inter-crystalline fractionation, mixtures and mineral reactions. Pp. 131–165 in: *Mixtures and Mineral Reactions* (J. Ganguly and S.K. Saxena, editors). Minerals and Rocks Series, Springer.
- Ganguly, J. and Tirone, M. (1999) Diffusion closure temperature and age of a mineral with arbitrary extent of diffusion: theoretical formulation and applications. *Earth and Planetary Science Letters*, **170**(1), 131–140.
- Ganguly, J., Tirone, M., Chakraborty, S. and Domanik, K. (2013) H-chondrite parent asteroid: A multistage cooling, fragmentation and re-accretion history constrained by thermometric studies, diffusion kinetic modeling and geochronological data. *Geochimica et Cosmochimica Acta*, **105**, 206–220.
- Gansser, A. (1977) The great suture zone between Himalaya and Tibet: A Preliminary account. Himalaya-sciences de la terra Colloques International, 7–10 December 1976, Editions du Centre National de la Recherche Scientifique, Paris, 268, pp. 181–192.
- Girardeau, J., Mercier, J. and Yougong, Z. (1985) Structure of the Xigaze ophiolite, Yarlung Zangbo suture zone, southern Tibet, China: Genetic implications. *Tectonics*, **4**(3), 267–288.
- Hackl, K. and Renner, J. (2013) High-temperature deformation and recrystallization: A variational analysis and its application to olivine aggregates. *Journal of Geophysical Research: Solid Earth*, **118**(3), 943–967.
- Hébert, R., Bezard, R., Guilmette, C., Dostal, J., Wang, C.S. and Liu, Z.F. (2012) The Indus–Yarlung Zangbo ophiolites from Nanga Parbat to Namche Barwa syntaxes, southern Tibet: First synthesis of petrology, geochemistry, and geochronology with incidences on geodynamic reconstructions of Neo-Tethys. *Gondwana Research*, **22**(2), 377–397.
- Hiraga, T., Anderson, I.M. and Kohlstedt, D.L. (2003) Chemistry of grain boundaries in mantle rocks. *American Mineralogist*, **88**(7), 1015–1019.
- Hiraga, T., Anderson, I.M. and Kohlstedt, D.L. (2004) Grain boundaries as reservoirs of incompatible elements in the Earth's mantle. *Nature*, **427**(6976), 699–703.
- Huot, F., Hébert, R., Varfaly, V., Beaudoin, G., Wang, C., Liu, Z., Cotten, J. and Dostal, J. (2002) The Beimarang mélange (southern Tibet) brings additional constraints in assessing the origin, metamorphic evolution and obduction processes of the Yarlung Zangbo ophiolite. *Journal of Asian Earth Sciences*, **21**(3), 307–322.
- Jenkin, G., Farrow, C., Fallick, A. and Higgins, D. (1994) Oxygen isotope exchange and closure temperatures in cooling rocks. *Journal of Metamorphic Geology*, **12**(3), 221–235.
- Kawasaki, T. and Ito, E. (1994) An experimental determination of the exchange reaction of  $\text{Fe}^{2+}$  and  $\text{Mg}^{2+}$  between olivine and Ca-rich clinopyroxene. *American Mineralogist*, **79**(5–6), 461–477.
- Lasaga, A.C. (1983) Geospeedometry: An Extension of Geothermometry. Pp. 81–114 in: *Kinetics and Equilibrium in Mineral Reactions* (S.K. Saxena, editor). Springer, New York.
- Lasaga, A.C. (1986) Metamorphic reaction rate laws and development of isograds. *Mineralogical Magazine*, **50** (357), 359–373.
- Lasaga, A.C. (2014) *Kinetic Theory in the Earth Sciences*. Princeton University Press, Princeton, New Jersey, USA.
- Liang, Y., Sun, C., and Yao, L. (2013) A REE-in-two-pyroxene thermometer for mafic and ultramafic rocks. *Geochimica et Cosmochimica Acta*, **102**, 246–260.
- Liermann, H.-P. and Ganguly, J. (2003)  $\text{Fe}^{2+}$ –Mg fractionation between orthopyroxene and spinel: experimental calibration in the system  $\text{FeO}$ – $\text{MgO}$ – $\text{Al}_2\text{O}_3$ – $\text{Cr}_2\text{O}_3$ – $\text{SiO}_2$ , and applications. *Contributions to Mineralogy and Petrology*, **145**(2), 217–227.
- Molnar, P. and Tapponnier, P. (1975) Cenozoic Tectonics of Asia: Effects of a Continental Collision. Features of recent continental tectonics in Asia can be interpreted as results of the India–Eurasia collision. *Science*, **189**(4201), 419–426.
- Nicolas, A. (1981) The Xigaze ophiolite (Tibet): a peculiar oceanic lithosphere. *Nature*, 294(5840): 414.

- Tang, M., Rudnick, R.L., McDonough, W.F., Bose, M., Goreva, Y. (2017) Multi-mode Li diffusion in natural zircons: Evidence for diffusion in the presence of step-function concentration boundaries. *Earth and Planetary Science Letters*, **474**, 110–119.
- von Seckendorff, V. and O'Neill, H.S.C. (1993) An experimental study of Fe-Mg partitioning between olivine and orthopyroxene at 1173, 1273 and 1423 K and 1.6 GPa. *Contributions to Mineralogy and Petrology*, **113**(2), 196–207.
- Yin, A. and Harrison, T.M. (2000) Geologic evolution of the Himalayan-Tibetan orogen. *Annual Review of Earth and Planetary Sciences*, **28**(1), 211–280.
- Yin, J., Xu, J., Liu, C. and Li, H. (1988) The Tibetan plateau: regional stratigraphic context and previous work. *Philosophical Transactions of the Royal Society of London. Series A, Mathematical and Physical Sciences*, **327**(1594), 5–52.
- Zhang, C., Liu, C.Z., Wu, F.-Y., Ji, W.-B., Liu, T. and Xu, Y. (2017) Ultra-refractory mantle domains in the Luqu ophiolite (Tibet): Petrology and tectonic setting. *Lithos*, **286–287**, 252–263.
- Zhukova, I., O'Neill, H. and Campbell, I.H. (2017) A subsidiary fast-diffusing substitution mechanism of Al in forsterite investigated using diffusion experiments under controlled thermodynamic conditions. *Contributions to Mineralogy and Petrology*, **172**(7), 53.

